FINITE ELEMENT MODELLING AND ANALYSIS OF RECOIL SPRINGS IN
AUTOMATIC WEAPONS

A THESIS SUBMITTED TO
THE GRADUATE SCHOOL OF NATURAL AND APPLIED SCIENCES
OF
MIDDLE EAST TECHNICAL UNIVERSITY

BY

HAKAN ZALOĞLU

IN PARTIAL FULFILLMENT OF THE REQUIREMENTS
FOR
THE DEGREE OF MASTER OF SCIENCE
IN
MECHANICAL ENGINEERING

JANUARY 2013

Approval of the thesis:

FINITE ELEMENT MODELLING AND ANALYSIS OF RECOIL SPRINGS IN AUTOMATIC WEAPONS

submitted by **Hakan ZALOĞLU** in partial fulfillment of the requirements for the degree of **Master of Science in Mechanical Engineering Department, Middle East Technical University** by,

Prof. Dr. Canan ÖZGEN _____
Dean, Graduate School of **Natural and Applied Sciences**

Prof. Dr. Süha ORAL _____
Head of Department, **Mechanical Engineering**

Asst. Prof.Dr. Gökhan O. ÖZGEN _____
Supervisor, **Mechanical Engineering Dept., METU**

Asst. Prof.Dr. Ender CİĞEROĞLU _____
Co-Supervisor, **Mechanical Engineering Dept., METU**

Examining Committee Members:

Prof. Dr. Suat KADIOĞLU _____
Mechanical Engineering Dept., METU

Asst. Prof. Dr. Gökhan O. ÖZGEN _____
Mechanical Engineering Dept., METU

Asst. Prof. Dr. Ender CİĞEROĞLU _____
Mechanical Engineering Dept., METU

Assoc. Prof. Dr. Serkan DAĞ _____
Mechanical Engineering Dept., METU

Prof. Dr. Yavuz YAMAN _____
Aerospace Engineering Dept., METU

Date: 30.01.2013

I hereby declare that all information in this document has been obtained and presented in accordance with academic rules and ethical conduct. I also declare that, as required by these rules and conduct, I have fully cited and referenced all material and results that are not original to this work.

Name, Last name: Hakan Zaloğlu

Signature:

ABSTRACT

FINITE ELEMENT MODELLING AND ANALYSIS OF RECOIL SPRINGS IN
AUTOMATIC WEAPONS

ZALOĞLU, HAKAN

M.Sc. Department of Mechanical Engineering
Supervisor: Asst. Prof. Dr. O. Gökhan ÖZGEN
Co-Supervisor: Asst. Prof. Dr. Ender CİĞEROĞLU

JANUARY 2013, 85 pages

As a tool for weapon designers, a finite element based analysis methodology is developed for estimating the mechanical behavior of the recoil spring during a firing cycle. All models are developed in LS-DYNA to be used in analysis to estimate the nonlinear force deflection characteristics and dynamic stress in the spring during a representative firing cycle. An experimental study is also performed to validate the finite element based analysis methodology. Modeling, analysis approach and modeling parameters and their effects on the accuracy of force-deflection characteristics and stress responses are obtained from finite element based methodology. Moreover, those effects are investigated via various simulated scenarios and comparisons are made between the results of analysis and actual experiments replicating some of the analysis performed.

Weapon designers should be able to estimate the spring parameters carefully in order to simulate the gun dynamics during the design phase. In addition, stress levels in the spring during the firing cycle should remain below the yield stress of the material. The designer sets the stiffness of the recoil spring by considering the rounds fired in unit time and also the desired recoil characteristics of the weapon to be designed. The recoil spring in a rifle is a long slender component, which is susceptible to buckling. Buckling behavior causes geometric nonlinearity in its deflection response. Therefore, the stiffness of the spring is really not a constant value, rather it is a relation that should be modeled as a function of deformation.

Keywords: Design of Recoil Spring, Geometric Nonlinearity, Large Deformations, Buckling of Helical Springs, Finite Element Analysis

ÖZ

SONLU ELEMANLAR METHODU İLE OTOMATİK SİLAHLARDA KULLANILAN İCRA YAYININ MODELLENMESİ VE ANALİZİ

ZALOĞLU, Hakan

Yüksek Lisans, Makina Mühendisliği Bölümü
Tez Yöneticisi: Yrd. Doç. Dr. Gökhan ÖZGEN
Ortak Tez Yöneticisi: Yrd. Doç. Dr. Ender CİĞEROĞLU

Ocak 2013, 85 sayfa

Bu çalışmada, tam otomatik silahlarda kullanılan icra yayının atış döngüsünde gösterdiği mekanik özelliklerinin anlaşılabilmesi için, sonlu elemanlar temelli analiz metodolojisi geliştirilmiştir. Modellerin tümü LS DYNA programında oluşturulmuştur. Yayın atım döngüsü esnasındaki ileri geri hareketi sırasında görülen lineer olmayan kuvvet deplasman ilişkisi ve yay üzerinde oluşan dinamik gerilimler gibi sonuçlara ulaşılmıştır. Sonlu elemanlar modelleme yaklaşımını doğrulamak için ve parametrelerin doğruluğunu anlayabilmek için, deneysel çalışma yapılmıştır. Belirli durumlar için analizde uygulanan koşullar, labratuvar ortamında uygulanmış ve deneysel sonuçlar, analiz sonuçları ile karşılaştırılmıştır.

Tam otomatik silahlarda kullanılan icra yayı, şarjörden dolu merminin alınmasından ve namluya sürülmesinden sorumludur. Merminin patlamasından sonra ortaya çıkan kuvvet, tüm kurma mekanizmasını geriye doğru hareket ettirir ve böylece atım döngüsü tekrar başa döner. Bu yay sayesinde silah, atış yapabilme kabiliyetini sürdürür.

Yay tasarımı yapılırken, oluşacak gerilimlerin akma mukavemetinden düşük olmasına dikkat edilmelidir. Silah tasarımcısı için önemli olan, yayın deplasman-kuvvet karakteristiği ve oluşacak gerilimlerdir. Deplasman-kuvvet ilişkisi, silahın atım sayısını belirleyen önemli bir faktördür.

Buna ek olarak, icra yayı ince uzun bir yapıda olup, burkulma hareketine müsait bir yapıdadır. Her ne kadar, tasarımlarda yayı kılavuzlayan bir çubuk kullanılsa da yayın burkulma hareketi engellenemez. Bu hareket de sisteme geometrik lineer olmayan bir özellik kazandırır. Bu durumda yay sabiti artık basit bir sabit olmaktan çıkar ve deformasyona göre değişen bir fonksiyon özelliği kazanır.

Silah tasarımcıları yay hesaplarını yaparken, geometrik lineer olmayan durumun da incelendiği ve hem gerilim hem yay karakteristiğini bulduran bir araca ihtiyaç duyarlar. Bu çalışma, silah tasarımcısına sonlu elemanlar modelleme yaklaşımı ile kullanılabilecek bir metodoloji sunar.

Anahtar Kelimeler: İcra Yayı Tasarımı, Geometrik Lineer Olmayan Durum, Yaylarda Yüksek Deformasyon, Sonlu Elemanlar Analizi, Yay Burulması

To My Family...

ACKNOWLEDGEMENTS

TABLE OF CONTENTS

LIST OF TABLES

LIST OF FIGURES

FIGURES

xiv

NOMENCLATURE

D .... Mean Diameter of Helical Spring

d .... Wire Diameter

p .... Pitch of Helical Spring

k .... Stiffness of Spring

F .... Axial Force On Spring

τ .... Shear Stress on Wire Section

m .... Mass of Bolt

K_w .... Wahl Factor

K_B .... Bergstrasser Factor

N_a .... Number of Active Coils

y_{cr} .... Critical Deflection For Buckling

L_o .... Free Length of Spring

λ_{eff} .... Effective Slenderness Ratio

α .... End-Condition Constant

G .... Shear Modulus

E .... Modulus of Elasticity

υ .... Poisson Ratio

R_G .... Gage Resistance

V_0 .... Gage Voltage

V_{ex} .... Input Voltage

GF .... Gage Factor

R_1, R_2, R_3, R_4 .... Wheatstone Bridge Resistances

$\varepsilon_1, \varepsilon_2, \varepsilon_3$ ....Corresponding Strains

VDC..Viscous Damping Coefficient

V_{rel}...Relative Velocity

DC...Exponential Decay Coefficient

μ_c..Contact Friction Coefficient

VDC..Viscous Damping Coefficient

FS...Static Friction Coefficient

FD..Dynamic Friction Coefficient

[C]..Damping Matrix

[K]..Stiffness Matrix

[M] .... Mass Matrix

α .... Alpha (Mass) Damping

β ....Beta (Stiffness) Damping

ξ_i...i^{th} Damping Ratio

CHAPTER 1

INTRODUCTION

Recoil spring is a vital part of the firing mechanism in an automatic rifle. It is responsible from maintaining the movement of the bolt inside the mechanism. Because of this motion, the cartridge is pushed into the firing chamber and after the bullet is fired, thrown out of the chamber and the bolt catches a new cartridge and drives it into the chamber again. This movement goes on as the finger of the user holds on the trigger until the ammo finishes.

When designing an automatic weapon, the recoil spring parameters should be determined carefully since it is directly connected to the dynamics of the firing mechanism and the general recoil characteristics of the weapon. Spring character sets the number of shots fired in a unit time, which is a design specification for the complete system.

Although there are conventional simple design formulae [1] for recoil springs, the actual mechanics of the recoil spring is relatively complex. Most dominant complexity comes from the fact that it is prone to buckling since it has a long and slender structure due to the geometric constraints inside the rifle. Generally, the recoil spring is positioned around a slender (guidance) rod inside the rifle, however, there is still some amount of buckling occurring this time associated with frictional contact with the guidance rod. Buckling phenomena imparts geometric nonlinearity into the spring character. Hence, the force-deflection relation is not a linear one, instead it is nonlinear.

Although there are lengthy and cumbersome analytical methods in literature [2], to analyze recoil spring mechanics, these studies do not consider the effect of buckling and interaction of the spring with its environment. For example in reference [2], useful and practical information about recoil spring design is depicted. However, these calculations can only give a rough estimate of the actual recoil spring dynamics since they are very simple and relies on many assumptions.

Since recoil spring is the key member in the weapon firing mechanism, design should guarantee that the maximum shear stress levels are below the strength limit and the designer can find the relation between force and deflection. In order to determine the force-deflection characteristics and stress levels in the recoil spring, weapon designers require a fast and reliable tool and methodology for analysis.

A good candidate is finite element method which can handle the large deformations and contact nonlinearities in the recoil spring during the firing process

In fact, main purpose of this thesis, is to develop a finite element analysis-based methodology for weapon designers by which the nonlinear mechanics of the recoil spring (i.e. force-deflection characteristics, buckling and geometric non linearities) and stress levels can be estimated. It is essential to mention that, there is no specific finite element modeling study on helical springs that are subjected to loadings as recoil springs experience. Hence, this thesis study is based on finding important parameters and making adjustments in finite element analysis for building a model of the recoil spring. In this work, numerous analysis runs are performed to see the parameter change effect on the force displacement character. An experiment is also performed to compare the results of the finite element analysis with the actual measured data so that the developed modeling and analysis procedure can be validated.

In the second chapter of the thesis, a literature survey is presented which gives general information about internal structure of the rifle with brief explanations of the functions of each component. Firing cycle and the role of the recoil spring in the firing mechanism is explained in detail. Finite element models used for analyzing helical spring mechanics are also presented in this chapter. In the third part of the thesis, finite element modeling and analysis procedures are developed for recoil springs. Model details such as boundary conditions, element types and analysis type are discussed. Models constructed in LS-DYNA are presented by changing several parameters to observe their effect on force displacement character.

In the fourth chapter, in order to see the modeling performance, an experiment is designed and performed on a sample helical spring. In this experiment, force deflection characteristics and stress on selected point are found. Experiment set up, applied boundary conditions and the methodology are also given in detail in this chapter.

In the fifth chapter, the helical spring used in the experiment is modeled in finite element environment and analysis parameters are adjusted in order to tune finite element model and analysis results to the experimental results.

CHAPTER 2

LITERATURE SURVEY

Literature survey is focused on four main topics. First, basic definition and structure of an automatic weapon and the purpose of the recoil spring are described. Secondly, conventional formulae used to analyze recoil springs widely in literature are given. In the third part, guidelines for finite element model construction of helical springs is given. Boundary conditions, element types and other important controls are shown. In the final part, experimental studies are presented.

2.1 FIRING CYCLE AND RECOIL SPRING

Automatic weapon or a machine gun refers to the guns which have the ability to fire rounds continuously until the rounds in the magazine finish. The energy necessary to maintain the cycle is supplied from the burning of propellant in the cartridge. Automatic weapons are classified as follows [3]:

- o   Mass locked weapons (Blowback weapons)
- o   Recoil operated weapons
- o   Gas operated weapons
- o   Semi rigid locking weapons
- o   Drum weapons(revolver cannons)

For the content of this thesis, first four items of the above list will be defined. Mass locked weapons use a heavy breech bolt which utilizes its inertia to support the cartridge. At the instant of firing, the breech bolt does not move or move slightly, so that the pressure drop behind the projectile is negligible. A typical example is the Thompson machine gun as shown in Figure 2.1. A cross sectional view is shown in Figure 2.2.

Figure 2.1. Thompson Gun [4]
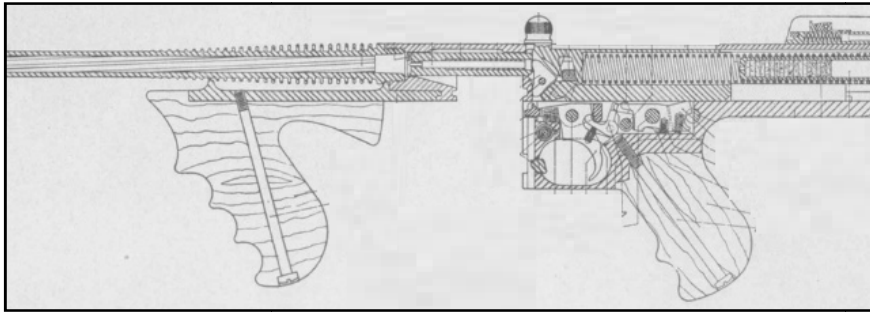
Figure 2.2. Thompson Gun Cross Section [4]

In recoil operated weapons, both barrel and the breech bolt are driven back by gas pressure. At first, the movement is synchronous then separate. By this mechanism, the breech bolt is post accelerated by a catapult effect. A typical example for this kind of machine is the MG-3.

In gas operated weapons, gas is transferred from barrel to the breech block and unlocking of breech block is necessary to restart the cycle. Most common product based on this approach is AK-47. Basic components are shown in Figure 2.3.

The firing cycle is explained on a gas operated weapon in below figures. The cycle consists of following steps[3]:

o   Trigger actuation: In this step, the user presses the trigger and the cycle starts. Then, the cartridge is pushed into the firing chamber by the bolt as shown in Figure 2.5 .
o   Breech bolt locked-ready to fire: Breech is locked in this step. Figure 2.6 should be examined.
o   Breech bolt unlocking: After the ignition, the bolt is unlocked and ready to slide backwards as shown in Figure 2.7.
o   Rejection of cartridge: While the mechanism is being restarted, the empty cartridge is repelled out of the weapon as shown in Figure 2.8
o   Ready to fire: The cycle is ready to start again as shown in Figure 2.4.

| Barrel | Gas Tap | Ammunition | Breech Assembly | Trigger Mechanism | Recoil Spring |

Figure 2.3. Basic Components in AK-47 [3]

Figure 2.4. Gas Operated Gun Ready to Fire [3]
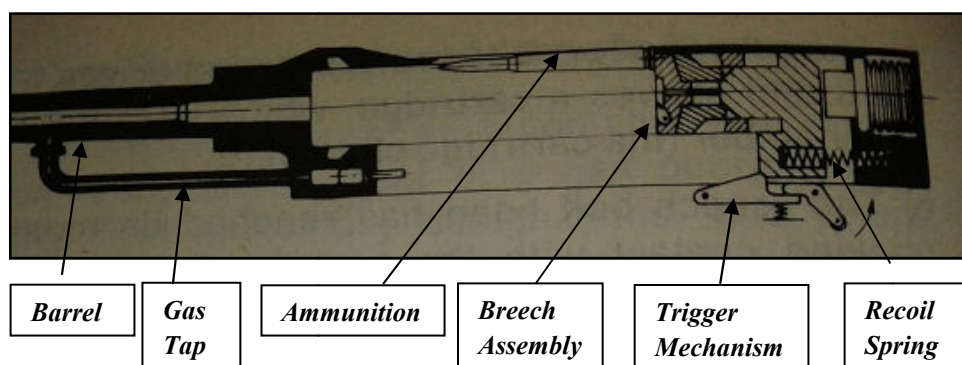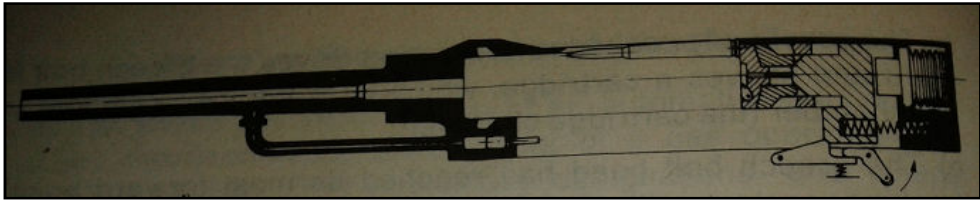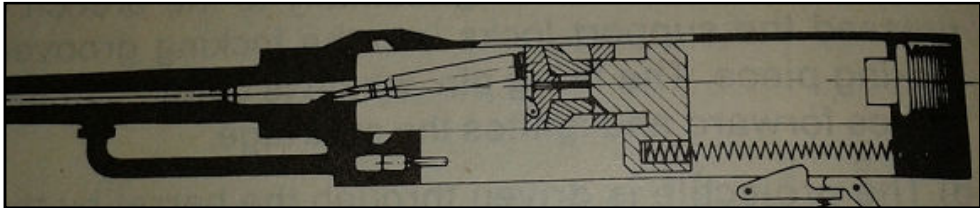

Figure 2.5. Trigger Actuation- Feeding of Cartridge to Firing Chamber [3]
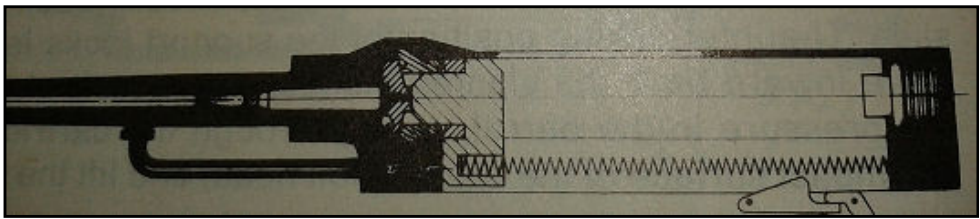
Figure 2.6. Breech Bolt Locked- Ready to Fire [3]
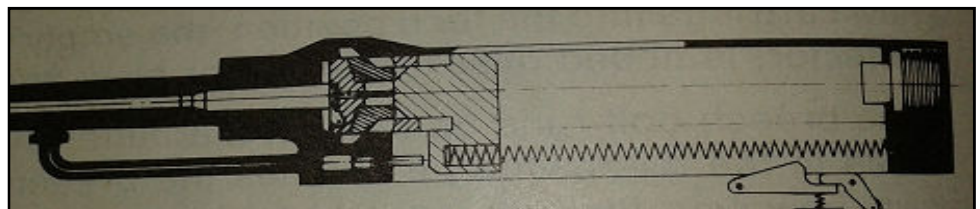
Figure 2.7. After Firing, Breech Bolt Unlocking Concluded [3]
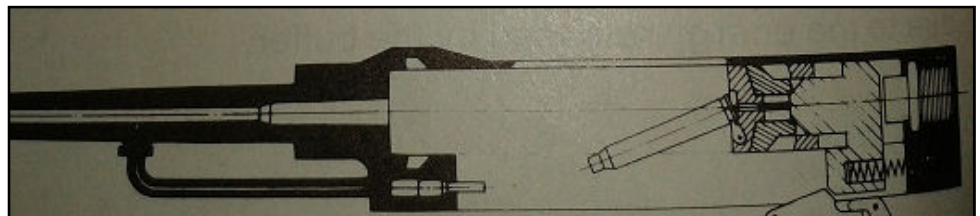
Figure 2.8. Cartridge Case Ejection [3]
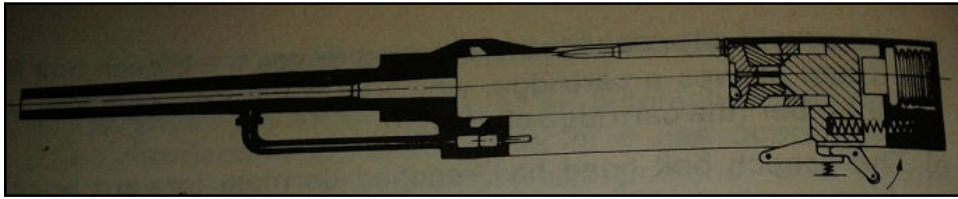
Figure 2.9. Cycle Start [3]

If Figures 2.5 to 2.7 are examined, it can be seen that the helical spring, which is connected to the breech assembly determines the dynamics of the breech. This spring is the recoil spring, or in other words, driving spring which maintains the firing cycle running.

For an automatic weapon, the rate of fire is high, around 500-600 rounds in burst fire mode disregarding heating of the barrel. That corresponds to 8 rounds in one second. For the weapon to fire so many rounds, the breech block has to move in the weapon up to a velocity of 1500 mm/sec or more depending on the round size and stroke. In semi rigid locking weapons, the movement of the bolt is delayed by some mechanisms. They are also called as retarded blowback weapons. As the pressure increases behind the muzzle, the bolt is unlocked and it can move backwards. G3 machine gun is a good example of this type. Figure 2.10 shows the internal firing mechanism inside the G3 rifle. Figure 2.10 shows the instant when the weapon is ready to fire. Figure 2.11 shows the backward movement of the bolt after unlocking. The recoil spring is connected to the bolt head carrier.
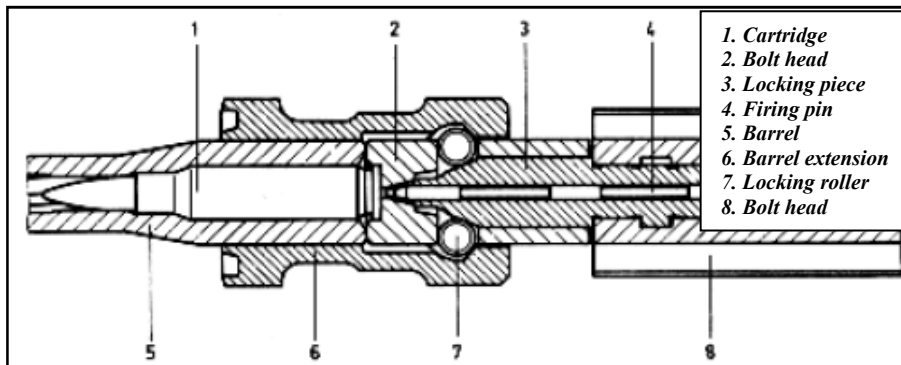
Figure 2.10. G3 Ready to Fire [5]
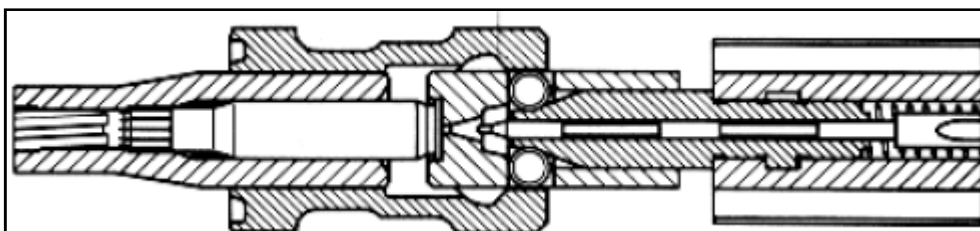
Figure 2.11. Bolt In Unlocked Position [5]

6

As all types of automatic weapons are considered, the cycle is maintained by the presence of recoil spring. Therefore, the spring should be able to keep its function. Stresses on the coil should be evaluated accurately. The number of rounds fired depends on the stiffness of the recoil spring.

When the dynamic equations for the bolt is written, the stiffness of the recoil spring appears in the equations. Hence, the stiffness should be found accurately as well. For a simple blowback type automatic weapon (see Figure 2.12), the mathematical model shown in Figure 2.13 can be used. Equation of motion of the bolt based on this model becomes:

$$m\ddot{x}(t) + kx(t) = F_{ignition} \qquad (2.1)$$

The equation of motion shows that, the position of the bolt depends on the stiffness character of the spring. However, the stiffness is not a constant term in reality. Figure 2.14 shows the recoil spring used in PKM machine gun in assembly.
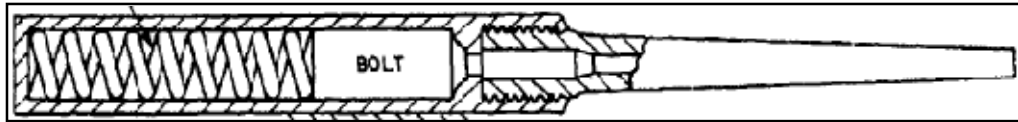
Figure 2.12. Schematic of Simple Blow Back Mechanism [3]
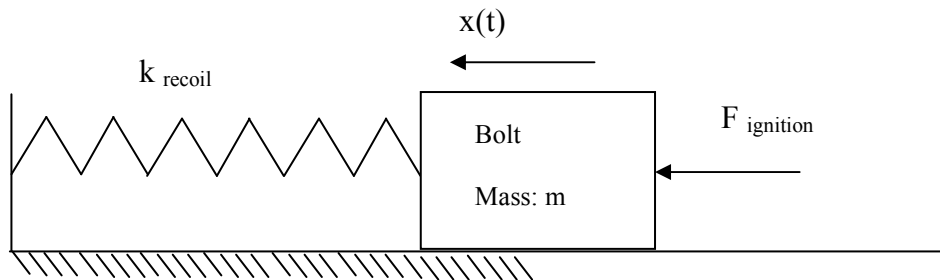
Figure 2.13. Mathematical Model of Simple Blow Back Mechanism

7

Figure 2.14. Recoil Spring In Assembly

Since the recoil spring is a long and slender structure it has a tendency to buckle. Buckling can easily be observed in Figure 2.14. In addition to this, the recoil spring experiences large deformations throughout its service life. Large deformation imparts mechanically nonlinear behavior as explained in Goncharenko's study [6].

2.2 CONVENTIONAL DESIGN OF RECOIL SPRING

There are numerous sources available in literature about designing a helical spring. The stress induced in a helical spring may be found by using Equation 2.2 [1]:

$$\tau = K_s \times \frac{8FD}{\pi d^3}, \tag{2.2}$$

where,

F: Force acting on the spring along the spring axis

τ: Shear stress in the wire cross section

D: Mean diameter

d: Wire diameter

$$K_s = \frac{2C+1}{2C}, \tag{2.3}$$

$$C = \frac{D}{d}, \tag{2.4}$$

8

In order to consider the effect of curvature in the spring, two correction factors are proposed by Wahl and Bergstrasser [1] as below:

$$K_w = \frac{4C-1}{4C-4} + \frac{0.615}{C},$$ (2.5)

and

$$K_B = \frac{4C+2}{4C-3},$$ (2.6)

For spring stiffness, the spring rate k is given as [1]:

$$k = \frac{d^4 G}{8D^3 N},$$ (2.7)

where,

G: Shear modulus

N: Number of active coils

(a)   (b)
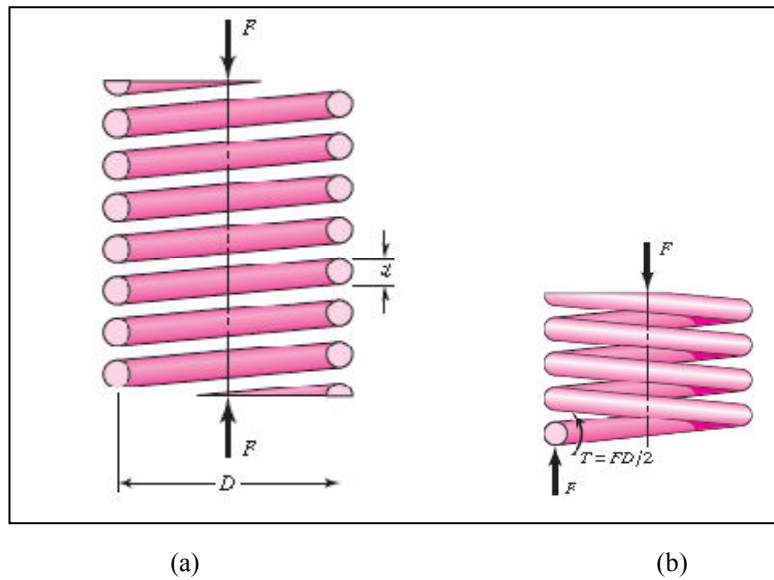
Figure 2.15. a)Section View of Helical Spring Under Loading[1],
b) Total Loading on the Section[1]

Buckling is an unstable mode for structural members that are under compressive stresses. Compressive loading causes sudden changes in the structure and may cause sudden failures. The main reason of buckling is that the compressive forces on the structure are not aligned [7]. For buckling behavior of a helical, the amount of deflection which causes buckling phenomena can be found by Equation 2.8 [1]:

$$y_{cr} = L_0 C_1' [1 - (1 - \frac{C_2'}{\lambda_{eff}^2})^{0.5}],$$ (2.8)

$$\lambda_{eff} = \frac{L_0 \alpha}{D},$$ (2.9)

$$C_1' = \frac{E}{2(E - G)},$$ (2.10)

$$C_2' = \frac{2\pi^2 (E - G)}{2G + E},$$ (2.11)

where,

L_0: Uncompressed length

α: End condition constant

D: Mean diameter

E: Modulus of elasticity

G: Shear modulus

λ_{eff}: Effective slenderness ratio

Above equations are the fundamental equations that are used in spring designs. Equations specifically derived for analyzing recoil springs can be found in [2] and [8].

2.3 FINITE ELEMENT MODELLING OF HELICAL SPRINGS

In literature, there are numerous studies based on helical spring modeling using commercial finite element software. Main modeling approaches are given in reference [9]. Three modeling approaches are given with specific boundary conditions and element types. One of the three approaches is used in this thesis. In this book [9], stress and stiffness results are also compared with each other and with an experiment for verification. In all three models, the spring's are compressed 295 mm's in axial direction. According to this reference, the stress induced in the wire cross section cannot be found by using simple beam elements in commercial software's. If used, a special post processing should be applied which involves manual coordinate frame transformations. If solid elements are used instead of beam elements, then both stiffness and stress results can be found. According to this reference, it is necessary to discretize one turn of the coil into 20 segments. The element length should be adjusted accordingly.

In the first modeling approach, the contact state between end turn and the seating is considered as a spring element with a stiffness constant of 5KN/mm, which can be considered as highly stiff. Figure 2.16 shows the first analytical model in Shimoseki et al's study [9]. As seen from this figure, all virtual nodes are connected to nodes on the helical spring with spring elements. Boundary conditions used in this model are shown in Table 2.1.The displacement of end turns are constrained by connecting those nodes on the spring with the virtual nodes that are placed on the z axis. The rotation of the system is constraint with the virtual node 5000 that is connected to the node on the end turn start.

For the second model, it is assumed that the deformation of the end turn is restrained by the seating surface. Figure 2.17 shows the modeling and Table 2.2 shows the boundary conditions.

In the final model, it is assumed that the end turn touches the mating surfaces from three points. Figure 2.18 shows the finite element model and Table 2.3 shows the applied boundary conditions.

Table 2.1. Boundary Conditions of Model 1[9]

Node Number	Displacement (mm)		
	x	y	z
1001 to 1020	0	0	0
2129 to 2148	0	0	-295
3000	0	0	0
4000	0	0	-295
5000	0	0	0
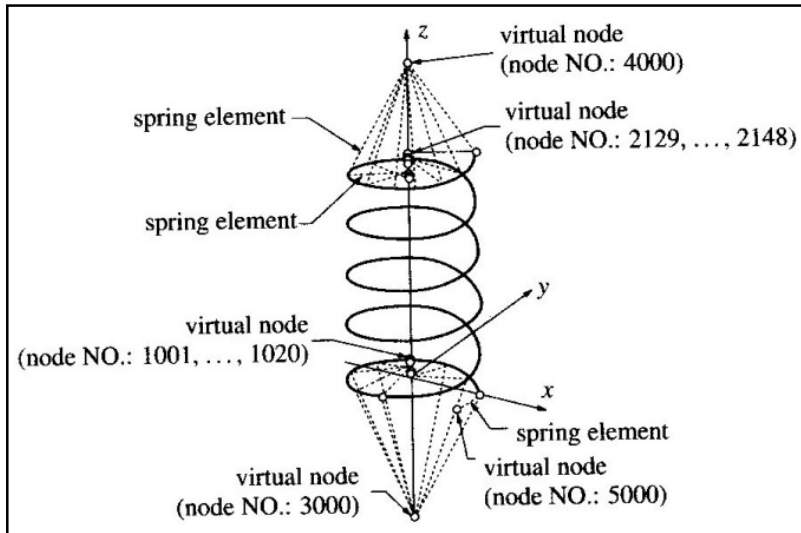
Figure 2.16. Analytical Model 1 [9]
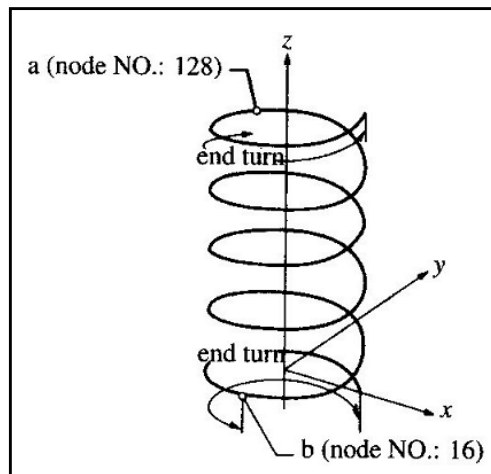
Figure 2.17. Analytical Model 2 [9]

Table 2.2. Boundary Conditions of Model 2[9]

Node Number	Displacement (mm)			Rotation(deg)		
	x	y	z	x	y	z
16	0	0	0	0	0	0
128	0	0	-295	0	0	0
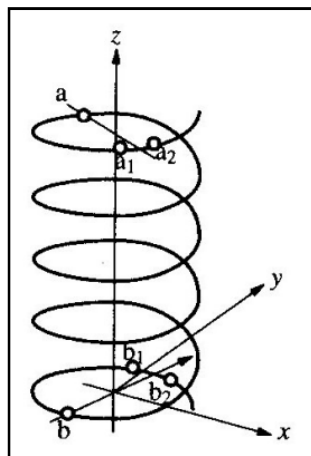
Figure 2.18. Analytical Model 3 [9]

Table 2.3. Boundary Conditions of Model 2[9]

Node Number	Displacement (mm)			Rotation(deg)		
	x	y	z	x	y	z
b	0	0	0	free	free	free
b₁	0	0	0	free	free	free
b₂	0	0	0	free	free	0
a	0	0	-295	free	free	free
a₁	0	0	-295	free	free	free
a₂	0	0	-295	free	free	free

When stress and stiffness results are compared among three models and the experiment, all models give close results. However, model 3 seem to be the most realistic and close to experimental verification. It is also emphasized that any contact of the coils with each other or any obstacle will cause non linear behavior in the force deflection character because of changing pitch angle.

Another useful study is performed by Lei et al [11]. They use a commercial vehicle's suspension, export it into CAD environment and then perform finite element analysis. During meshing, 3D solid elements with 8 nodes and hexahedral shape are used. It is important to note that the meshing is done in a sweep pattern. The spring is compressed with a force that is applied on a fictitious plane which represents the mating surface. This is an approach similar to the third approach in reference [9]. Figure 2.19 shows the original and deformed spring. Then an experiment is performed to find the stiffness of the spring and finally it is compared with the finite element analysis solution.
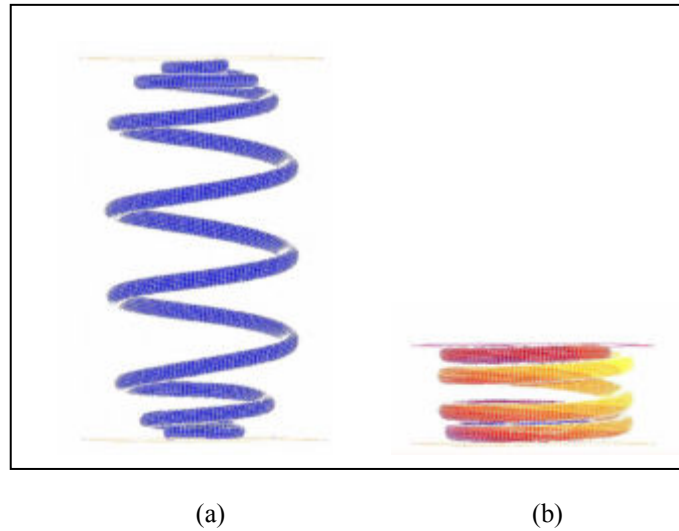
Figure 2.19. (a) Before Force Application, (b) After Force Application [11]

Husselman [12] elaborated on spring modeling in order to verify valve train dynamics in engines. Helical spring is modeled in a piecewise manner because end condition is selected as squared and ground. Then, the solid model is sliced into pieces in order to add contact elements between coils. The analysis is performed in PATRAN program by using solid wedge elements. During meshing, one turn is divided into segments corresponding to 15 degrees and the coil diameter is divided into 12 segments. Figure 2.20 shows the modeling approach. In order to simulate coil contact, contact elements are positioned between coils as shown in Figure 2.21. Then, stiffness character of the spring is derived. Gap elements detect contact and can apply different stiffness values according to the contact state.
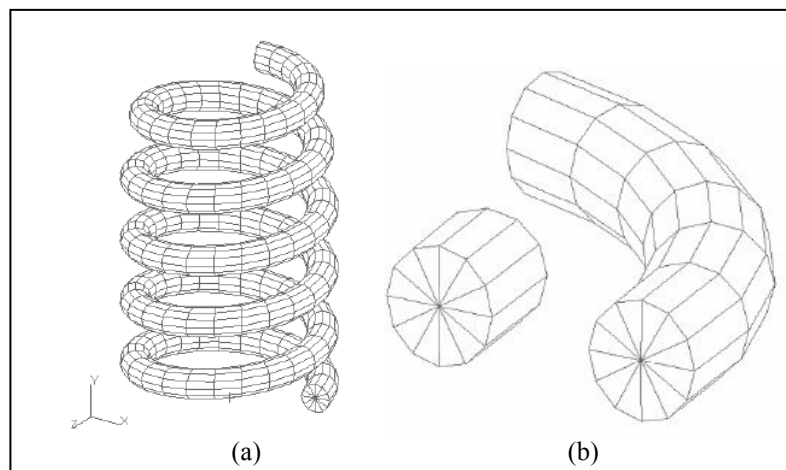
Figure 2.20. (a)Meshed Valve Spring, (b) Coil Cross Section[12]
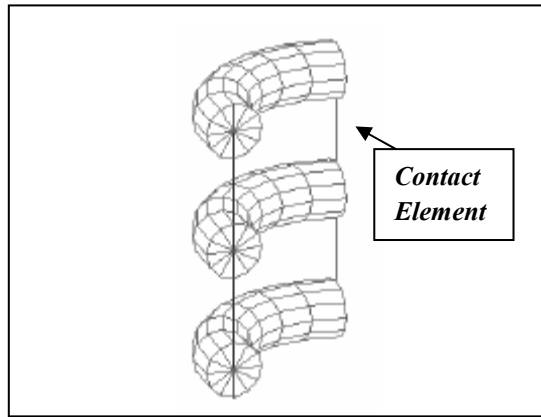
Figure 2.21. Gap-Contact Elements [12]

Mulla et al. [13] elaborated on finite element modeling of a helical spring that is used in a freight vehicle in India. In the study, a helical spring is modeled in ANSYS program with two different element types, namely, tetragonal shaped solid 187 and hexagonal shaped solid 186 elements. The meshing is done using free-mesher option. In addition to this, a convergence analysis is performed to investigate which element size to use. Then a force is applied from one end turn and maximum shear stress on the inside of the coil is searched for. Similar maximum shear stresses are found almost in every coil except the end turns. Figure 2.22 shows the meshed solid model and Figure 2.23 shows the maximum shear stress distribution.
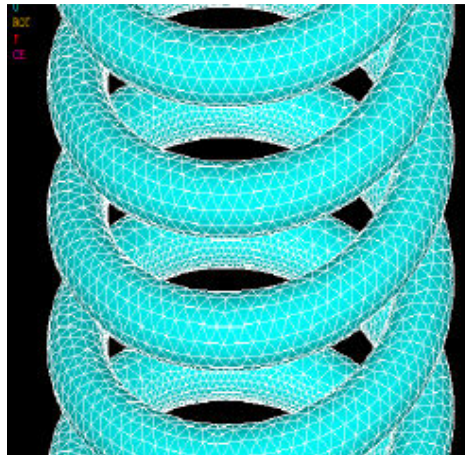
Figure 2.22. Meshed Solid Body [13]

Figure 2.23. Shear Stress Distribution [13]

Prawato et al. [10] worked on stress distribution in automotive suspension springs. They used 3D linear beam elements to model the spring and gap elements to model the coil and seating contact and contact between coils. Since beam elements are used during modeling, an in house post processing code is generated to find the stresses. Von Mises stresses in the wire are found. Figure 2.24 shows the finite element model that is used in Prawato's work which is composed of linear beam elements.
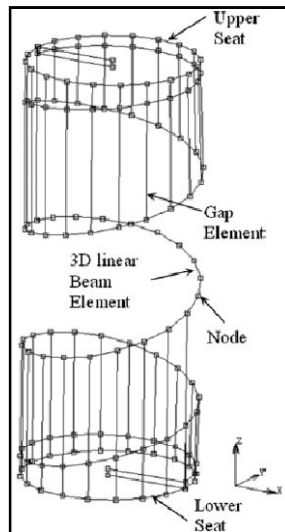
Figure 2.24. Modeling Approach Of Prawato et al.[10]

2.4. EXPERIMENTAL STUDIES ON STRESS DETERMINATION IN HELICAL SPRINGS

Since the purpose of this thesis is to determine a modeling methodology for recoil springs, there is a need to also verify the proposed modeling approach. One way of verifying the model is to compare results with experimental ones. Hence, this section is devoted for experimental studies performed on the helical springs. Determining the strain by using strain gages or photo elasticity is quite common. Strain gage measurements are discussed in the content of this section. Experimental stress measurements are performed on helical springs and results are presented. It is important to realize the type and orientation of the gages that are used. Besides it is important to notice the location of the gauges.

Keller and Gordon [19] worked on a helical spring that is subjected to bending. In their study, a helical compression spring is loaded with a moment as shown in Figure 2.25. Then in the experiment, four one directional strain gages are bonded on the helical spring as shown in Figure 2.26. Gages are located on the cross section quadrants. Experimental results are compared with a finite element model which gives the Von Mises stresses as shown in Figure 2.27. The finite element model is constructed in ANSYS program by applying displacements which does not cause any yield in the member.
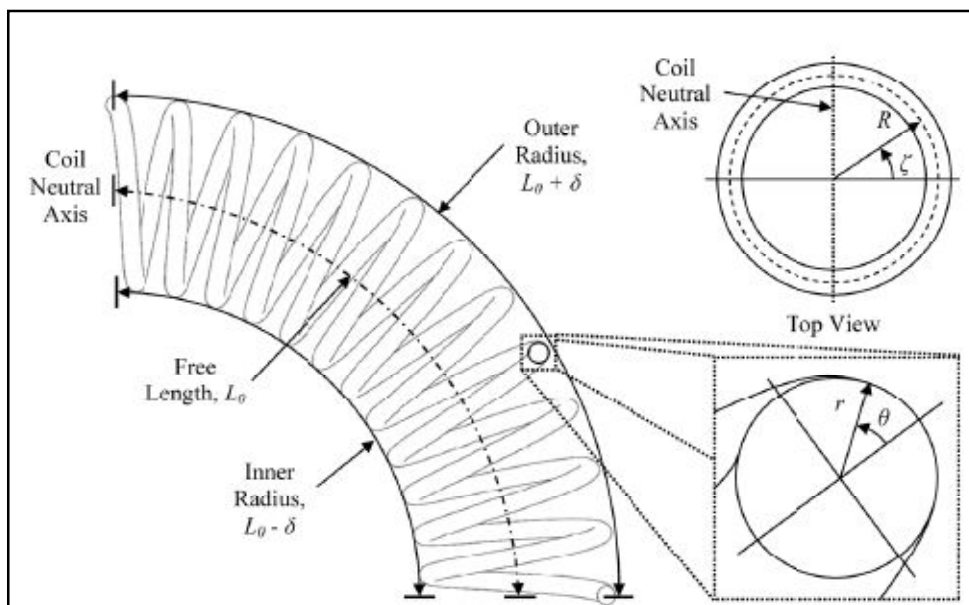
Figure 2.25. Helical Spring Under Bending [19]
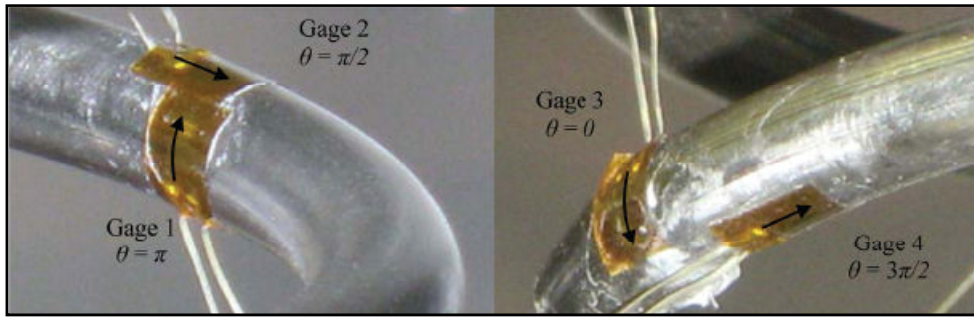
Figure 2.26. Strain Gage Bonding[19]
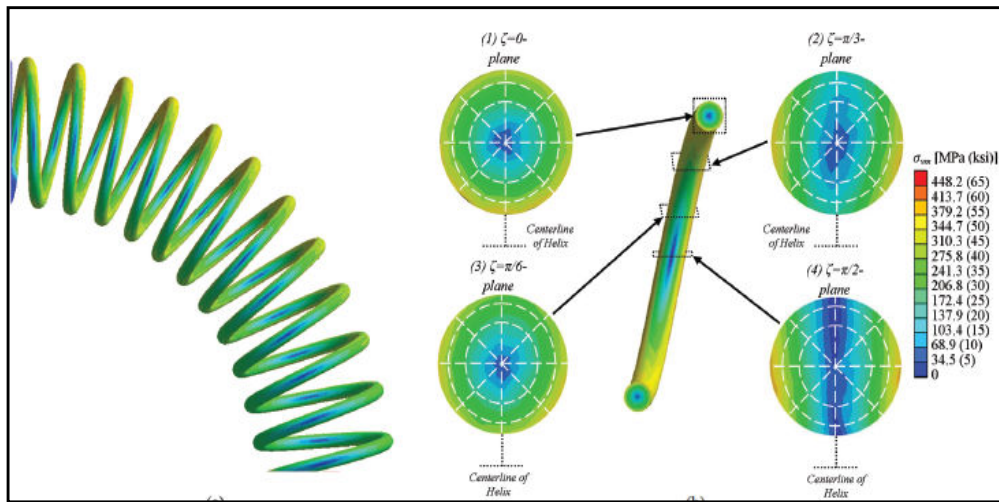
Figure 2.27. Finite Element Analysis Results[19]

A valuable study was conducted by McWilson [14]. In this study, it is aimed to specify the performance of helical compression spring in a compressor during the stopping motion. Some life tests are performed and strain gages are located on positions where there is failure. Total of three strain gages are applied on the inner surface of the coils as shown in Figure 2.28. Then shear stresses are found from those readings for an applied displacement to the spring.
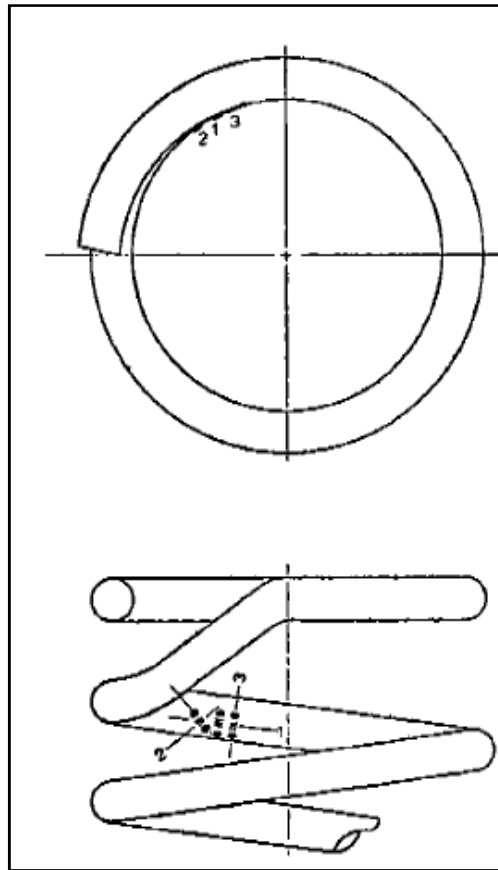
Figure 2.28. Helical Spring Strain Measurement [14]

Another simple study is being repeated in Iowa State University as a laboratory tutorial [20] . The experiment aims to show the stresses that are produced due to combined effect of torsional and axial loading in a helical spring. A three element strain gage rosette is bonded to the internal surface of the helical spring and the strains are recorded. Then they are converted to stresses by using theoretical relationships. Finally they are compared with the results obtained from analytical methods.

Throughout this chapter, the definition and purpose of a recoil spring in a automatic weapon is discussed. Finite element studies on modeling of a helical spring are also mentioned and experimental studies are investigated. Based on the gathered information, a finite element model of the recoil spring is developed in the next chapter.

CHAPTER 3

FINITE ELEMENT MODELLING AND ANALYSIS OF RECOIL SPRING

In order to develop the finite element model of a recoil spring, LS DYNA environment is chosen. For the finite element analysis to be performed, there are many parameters to be selected in LS DYNA software. Important parameters are discussed in the following sections with specific applications on selected springs which show the effect of each parameter on the results. Throughout this part of the thesis study, parameter effects on recoil spring finite element modeling such as friction, contact, damping, mesh size and boundary condition are investigated. For this purpose, shorter sample spring models are used to decrease analysis time. Properties of the models are shown in every section.

As shown in Figures 2.13 and 2.14, the recoil spring is guided with a (guidance) rod which prevents excessive buckling and the mechanism can be modeled as a single degree of freedom system. Since there is contact between rod and the spring, the analysis performed should be nonlinear. Contact itself is a nonlinear phenomena because the stiffness matrix changes continuously as contact is detected. Besides, buckling also results in a nonlinear behavior.

As the test sample, a recoil spring which has almost the same properties as the recoil spring in G3 rifle is used. Properties of the model are shown in Table 3.1.

Table 3.1. Properties of the Recoil Spring That is Used in Dynamic Analysis

Property	Value
d(mm)	1.5
D(mm)	11
p(mm)	10
L_0(mm)	400
G(GPa)	76.9
Na	40
Material	AISI 1040
End-Condition	Plain-Plain
E(GPa)	193
υ	0.3
C(N/mm)	1.1

3.1 FINITE ELEMENT MODEL CONSTRUCTION STEPS FOR THE RECOIL SPRING

As mentioned in previous section, this section focuses on the definition of necessary steps and points to keep in mind when constructing a finite element model for the recoil spring in LS DYNA software.

3.1.1 GEOMETRY CONSTRUCTION

First to mention is the physical structure of the model. It is necessary to construct a geometry as in shown in Figure 2.14. The geometric model of the spring is generated in ProEngineer CAD program. End turns of the spring are modeled as free-free with the geometrical parameters given in Table 3.1. The CAD model is shown in Figure 3.1. After defining the geometry, it is exported to LS DYNA program. After exporting the geometry, it is necessary to model a rod through the center of the helical spring. For the breech block which hits the spring, a rectangle with a bore on the rod axis is required. If not, as the block progresses into the spring and deforms it, the rod will touch the block and stop its movement. Figure 3.2 shows the physical structure of the model. This model will be called as "Collision Model" hereafter. If inertial effects are to be considered then it is essential to use this model with an explicit solver. The guiding rod and the breech block are modeled in LS DYNA. Apart from this model, another model is also constructed. This model does not include the effect of breech block. Figure 3.3 shows the physical structure. This model will be called as "Simple Spring Model" hereafter.
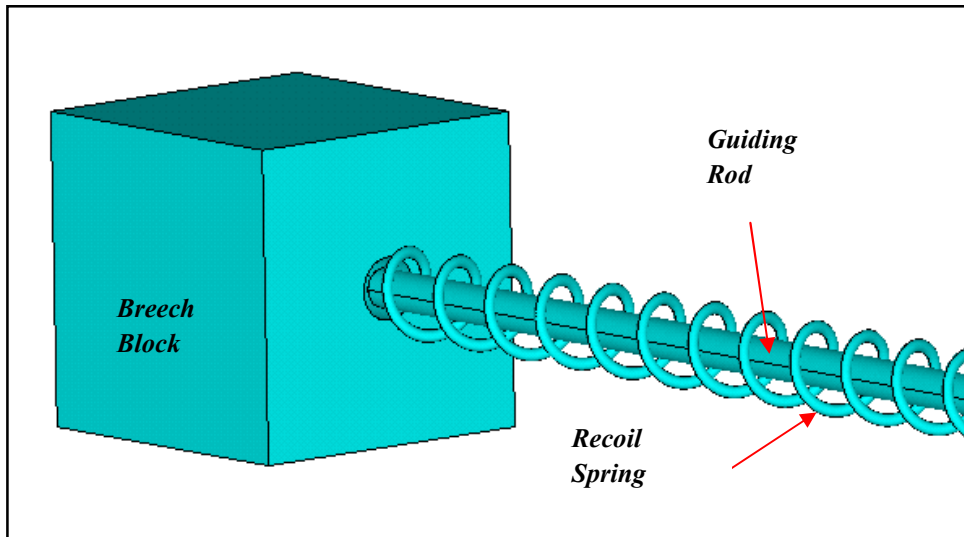

Figure 3.1. Helical Spring CAD Model

Figure 3.2. Physical Structure of the Model (Collision Model)

22
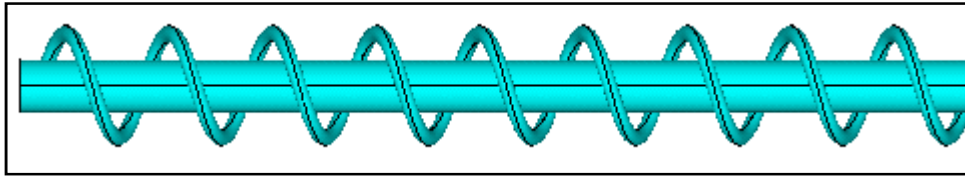
Figure 3.3. Physical Structure of the Model (Simple Spring Model)

The Collision Model can provide the user a means to apply velocity inputs directly to the breech block or if the internal pressure inside the barrel is known, to apply a time dependent pressure or force distribution. Since the mass of the block is also considered, all inertial effects are included inside this model.

Using the Simple Spring Model, displacement, force and velocity inputs can be applied to the helical spring through the nodes located at the free ends. It is important how the nodal degrees of freedoms are set. Boundary conditions will be explained in detail in further chapters.

Helical spring models with different geometric properties can be created by using these modeling approaches. In order to investigate effects of different model parameters, models other than G3 recoil spring are also created, which are shown and explained in further sections.

3.1.2 MESHING

After completing the physical construction of the G3 recoil spring model, it is necessary to create nodes and elements for the analysis to proceed. Therefore, the spring is meshed with SOLID 164 type elements in LS-DYNA. As name implies, this element type is used for modeling solids in the program. It involves eight nodes with x, y and z degrees of freedoms for translations, velocity and acceleration. Figure 3.3 shows the general structure of the element. Meshing of the helical spring is performed by using sweep mesh function.

While meshing, it is necessary to define an edge length. Edge length determines the size of the elements, hence larger edge length inputs create larger elements or vice versa. It is required to make successive analysis for the output of interest for different edge lengths and determine the edge length accordingly before making a dynamic analysis (convergence analysis).

Figure 3.4. SOLID 164 Type Element [26]

23

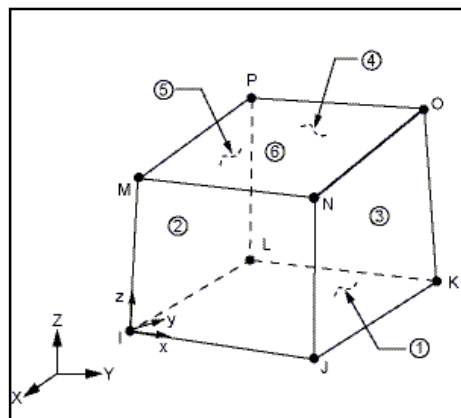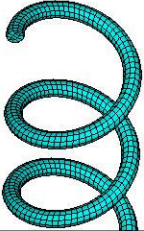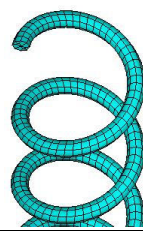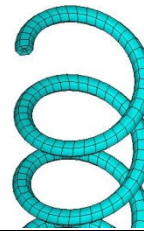In order to illustrate this, four models are constructed with four different edge lengths and the static linear stiffness results are compared with the results obtained by analytical methods (i.e. obtained by using Equation 2.7). Finite element analysis results shown in Table 3.2 are obtained after making linear static analysis. The boundary conditions of those models are applied as shown in Section 3.1.3. The G3 recoil spring with properties described in Table 3.1 is compressed by 5 millimeters. Results are shown in Table 3.2.

Table 3.2. Edge Length Effect On Result

MODELS				
Edge Length	0.5	0.7	0.9	1.2
FEA Stiffness Result (N/mm)	1.06	1.06	1.05	1.04
Analytical Result (N/mm)	1.1	1.1	1.1	1.1
Difference With Respect to Analytical Result(%)	-3.6	-3.6	-4.5	-5.5

When Table 3.2 is investigated, it is seen that finite element analysis results are very close to results obtained by analytical methods. Before making a dynamic analysis, it is important to check edge length and find an optimum value for accuracy and analysis time. For the analysis, although edge length of 1.2mm seems to be an optimum choice, for this edge length, the circular cross section has changed to almost a square section. This may cause problems in contact definitions and stress evaluations. Hence, edge length of 0.9mm is used for the analysis, which forms a cross section much more resembling a circle.

For the scope of this study, an edge length of 0.9 mm is used. Smaller values requires higher computational resources and longer computation time per analysis (nonlinear ones). Besides, the amount of discretization mentioned in Section 2 is also satisfied (it was stated that for a proper analysis of an helical spring, at least 20 segments should exist in one rotation of a coil. For an edge length of 0.9 mm the segment number is 36 for one complete turn of the coil of the G3 recoil spring).

While creating the finite element meshes of the Collision Model, the breech block and the guiding rod are modeled as rigid parts . Similarly, for the Simple Spring Model, guidance rod is modeled as rigid. By doing so, the amount of analysis time is reduced for both models. In LS-DYNA, the nodal degree of freedoms for a rigid body are accumulated at the center of mass of

the structure. Hence, no matter how many nodes exist, the rigid body may have 6 degree of freedoms at most.

3.1.3 BOUNDARY CONDITIONS

Boundary conditions effect the results of the analysis directly. Hence they are essential in a finite element analysis for finding accurate results. In literature survey chapter, three modeling approaches were presented which were discussed in [2]. In this section, third modeling approach of the three is applied on the spring.

First of all, one turn at the ends is selected to be fixed and the other is selected for compression. Figure 3.5 shows the application of the boundary conditions for fixing the geometry. The first node to be selected is node A. Then a virtual line is drawn from this node to the center of the spring axis to find the node that has an angle of 180 degrees with node A along the helix. This new node is the reference node for the remaining nodes. Finally, remaining two nodes are selected such that they are at equal angle to this reference node. For the other end, if the model is simple spring type, a similar node selection as shown in Figure 3.5 is done to apply the boundary conditions. On the other hand, if the geometry is representing Collision Model, the initial condition is given to the breech block as initial velocity.
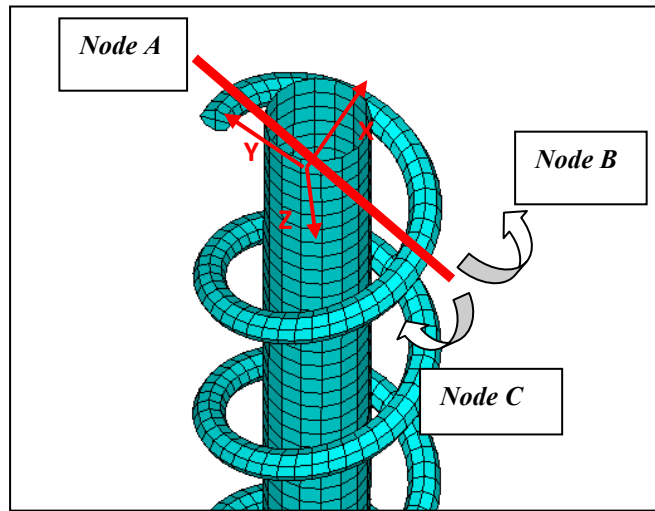
Figure 3.5. Boundary Condition Application For Fixing the Spring

It is important to set the boundary conditions for the nodes on which boundary conditions are applied. By using the spring with the properties given in Table 3.3, a model is constructed and displacement time input is applied as shown in Table 3.4. Application nodes are free to move in every direction. The physical structure of the constructed model is shown in Figure 3.6:

Table 3.3. Constructed Model Properties

Property	Value
d(mm)	1.5
D(mm)	11
p(mm)	10
L_0(mm)	400
G(GPa)	76.9
Na	40
Material	AISI 1040
End-Condition	Plain-Plain
E(GPa)	193
υ	0.3
C(N/mm)	1.1

Table 3.4. Applied Boundary Condition

Displacement (mm)	Time (sec)
0	0
-10	0.01
-15	0.02
-30	0.03
-40	0.05
-50	0.07
-50	0.08
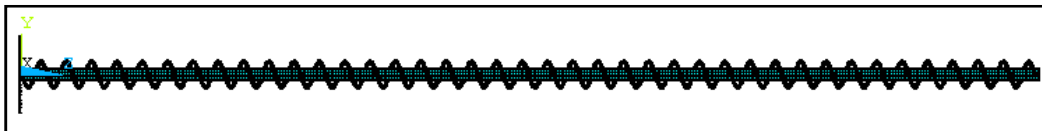
Figure 3.6. Physical Structure of the Model

The analysis is performed in LS DYNA just to check if the selected boundary conditions give consistent results with the results of the analytical solution. The only parameter of concern is the degree of freedom of the nodes. The analysis is performed without considering the effect of friction or damping. However, in order to observe buckling of the coil and prevent penetration between rod and the spring, large deformation effects are on and single surface contact is selected for this analysis. Contact is explained in next section.

As dynamic analysis is performed, it is seen that, there occurs a rotary motion because of unconstraint degree of freedom in x and y directions for the nodes on which displacement boundary condition is applied. This motion decreases the reaction force amplitudes obtained from the fixed nodes. Figure 3.7 shows the force-time relation for this boundary condition. As Figure 3.7 is observed, it is seen that force magnitudes are very low when compared to analytical results. As seen in Table 3.3, the stiffness of the spring is 1.1 N/mm which makes a force around 55 N for 50 mm of deformation. However, Figure 3.7 does not state that. It is obvious that, force amplitudes are low. Hence another model is constructed by adding x and y constraints on displacement applied nodes to see the effect of additional constraints. The boundary condition is changed to a more steady pattern as seen in Table 3.5. After application of this new boundary condition, force amplitudes increased significantly to the analytical force values as shown in Figure 3.8. For a given displacement of 100 mm, the required force should be around 110 N. By this boundary condition application, order of magnitudes are close. Hence for a simple spring type model, it is required to leave translational degree of freedom to the moving nodes and keep the rest as fixed in order to have a realistic model.
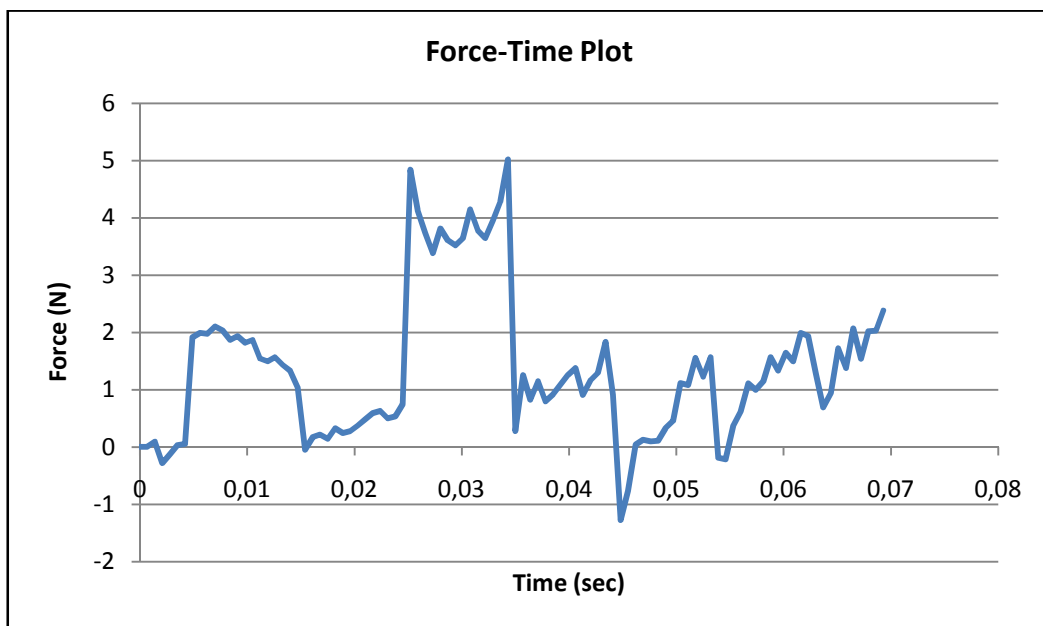
Figure 3.7. Force-Time Plot With Boundary Condition X-Y Free

27

Table 3.5. Applied Boundary Condition

Displacement (mm)	Time (sec)
0	0
-60	0.01
-100	0.02
-100	0.03
-100	0.05
-100	0.07
-100	0.08
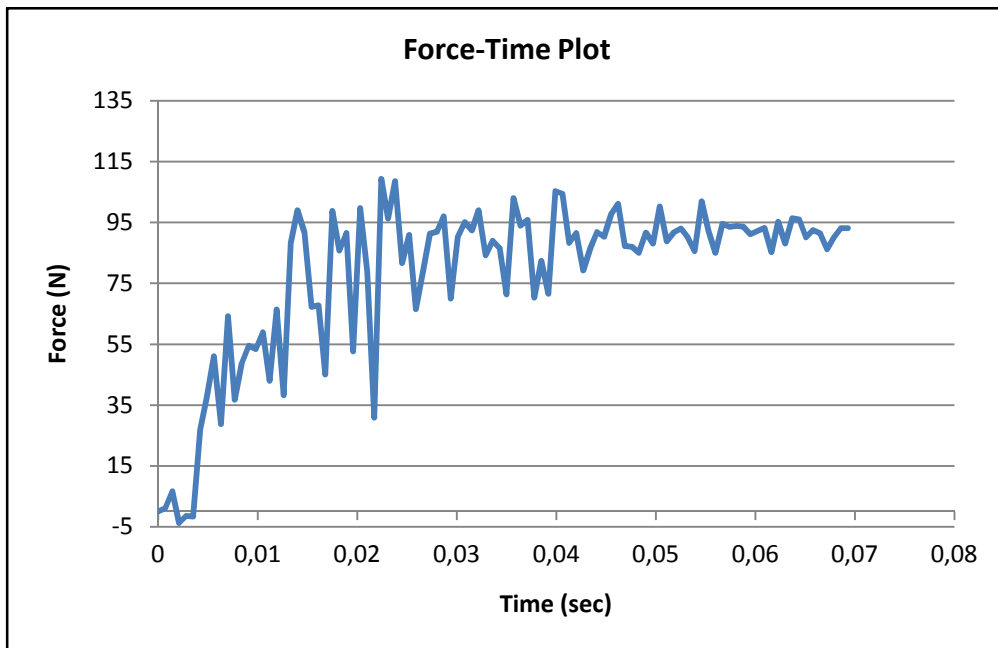
Figure 3.8. Force-Time Plot With Boundary Condition X-Y Fixed

3.1.4 CONTACT DEFINITION

In LS DYNA, there are many ways to determine the contact. One of the widely used contact algorithm is the "single surface contact". In this algorithm, whenever external surface of one body contacts itself or external surface of another body, contact is established. The algorithm searches for penetration in the external surfaces [21]. The strength of the algorithm comes from the ease of use. It is used extensively when the contacting bodies are not known beforehand or there is excessive deformation. Common application areas are crash and impact analysis in which the contacts are not known initially. In this algorithm, the user is not forced to select a target and a contact body. Determination of contact and target is also automatic. Self contact problems can be solved by this method. Figure 3.9 shows a self-contact problem in which single surface contact algorithm is used.
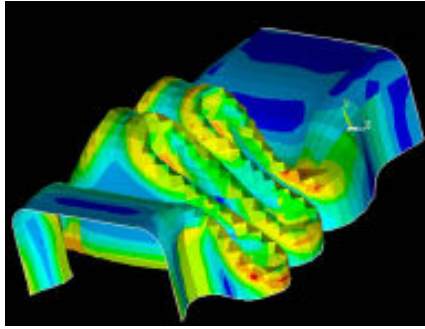
Figure 3.9. Self Contact Problem [22]

Although single surface contact definition is simple and widely used, there are some drawbacks. This algorithm automatically releases the contact if a node penetrates more than 40% of the thickness of the contacted element. This causes problems if the contacting parts are thin or the materials are soft such that they have low stiffness values. Moreover, high velocity impacts are also potential problem for this contact type. These conditions may lead to node penetrations more than 40%. Hence, the program cannot detect contact and materials will pass through each other. Contact nodes can be trapped behind the target surface [22].In the model constructed for this thesis, there are no such problems since the rod is modeled as a rigid solid body, not as a thin surface.

Single surface contact uses the penalty method to model contact behavior. Penalty method basically locates a spring between the contacting bodies. The spring stiffness is called contact stiffness and the amount of penetration is called the contact penetration. As soon as the contact is detected, the spring starts to apply a force that is proportional to amount of penetration. Those two terms are not physical, however they are required to solve contact problem. Figure 3.10 shows the contact spring between contacting bodies [22].

Figure 3.10. Contact Parameters Representation

For contact force to occur, there should be some amount of penetration. However, physical bodies do not interpenetrate each other. Hence, the following conditions should be satisfied for a realistic and highly accurate analysis:

- o   Penetration should be small.
- o   Contact stiffness should have a high value.

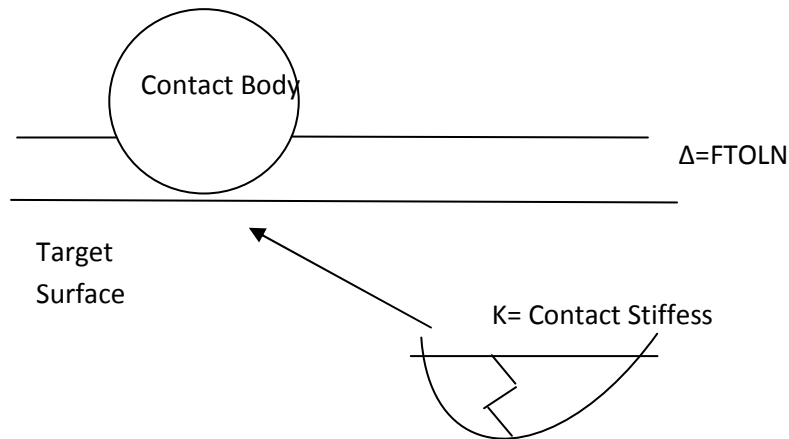LS-DYNA automatically defines the spring stiffness values by using the material properties of the contacting bodies. Hence, realistic material properties should be used during modeling. For the contact definition to be made, all parts are defined as part in the program. Contact is established between parts. While defining the contact, the user can define some amount of damping to the system. In reference [23], it is said that undesirable oscillation in contact can be reduced by applying some amount of damping, which is called as viscous damping coefficient (VDC). This damping is applied perpendicular to the contacting surfaces. The viscous contact damping (VDC) is defined in percentage of the critical damping such that 20 implies 20% of the critical damping.

In order to see the effect of contact damping, a simple spring model is constructed with the properties as shown in Table 3.6. This new spring model is selected to be simple and short in order to make successive trials in small amount of time.

The spring is compressed by the force given in Table 3.7. Forcing is applied to only one node in order to force the spring to touch the guiding rod and guarantee contact between spring and the rod to occur. Figure 3.11 shows the constructed model. The application point of the force is shown with a white square. This node is on the tip of the final turn. This model is meshed with SOLID 164 elements with edge length of 0.9mm. Properties of the spring are shown in Table 3.6. Boundary conditions are applied as described in Section 3.1.3. The analysis is repeated for different values of contact damping such as 3%, 15%, 40% and 80%.

Table 3.6. Short Spring Model Properties

Property	Value
d(mm)	1.5
D(mm)	11
p(mm)	10
L_0(mm)	50
G(GPa)	76.9
Na	6
Material	AISI 1040
End-Condition	Plain-Plain
E(GPa)	200
υ	0.3

Table 3.6 (cont'd)

C (N/mm)	8

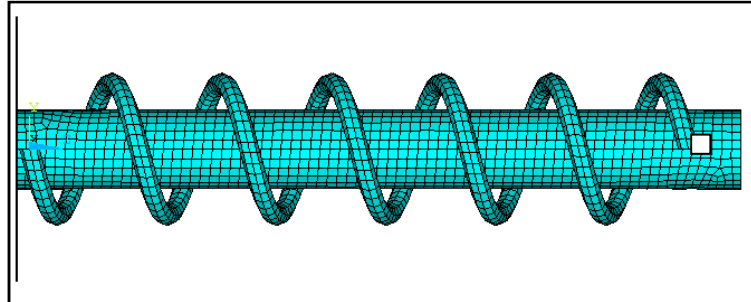**Figure 3.11.** Constructed Model To Investigate VDC Effect

Table 3.7. Applied Forcing on the Model

Time (sec)	Force (N)
0	0
0.01	3
0.05	5
0.06	5
0.1	5
0.13	5

After application of those forces, reaction forces on the axial direction are extracted from the output for the each of the three nodes that were fixed. Then they are processed and added to find the total reaction force in the compression direction. Figure 3.12 shows the effect of VDC on the reaction force. Contact phenomena occurs in an oscillatory manner since contacting surfaces interpenetrate each other, then some restoring force is applied by the contact spring to the bodies in order to diminish the interpenetration. This cyclic motion continues as contact is sensed.

As seen in Figure 3.12, applying VDC decreases the amount of oscillations that are caused because of contact between the rod and the spring. As Figure 3.12 is further observed, there are no oscillations before contact and reaction forces follow the applied force. However, as soon as contact occurs, oscillations start. Hence it is required to define some amount of contact damping in order to decrease the amount of oscillations. In reference [23], it is stated that, contact damping reduces the high frequency oscillation of contact forces in crash or impact simulations. Those oscillations are the ones that exist normal to the contact surfaces. Besides, it is said that, VDC can be selected as 20 or less for similar metals contacting each other.
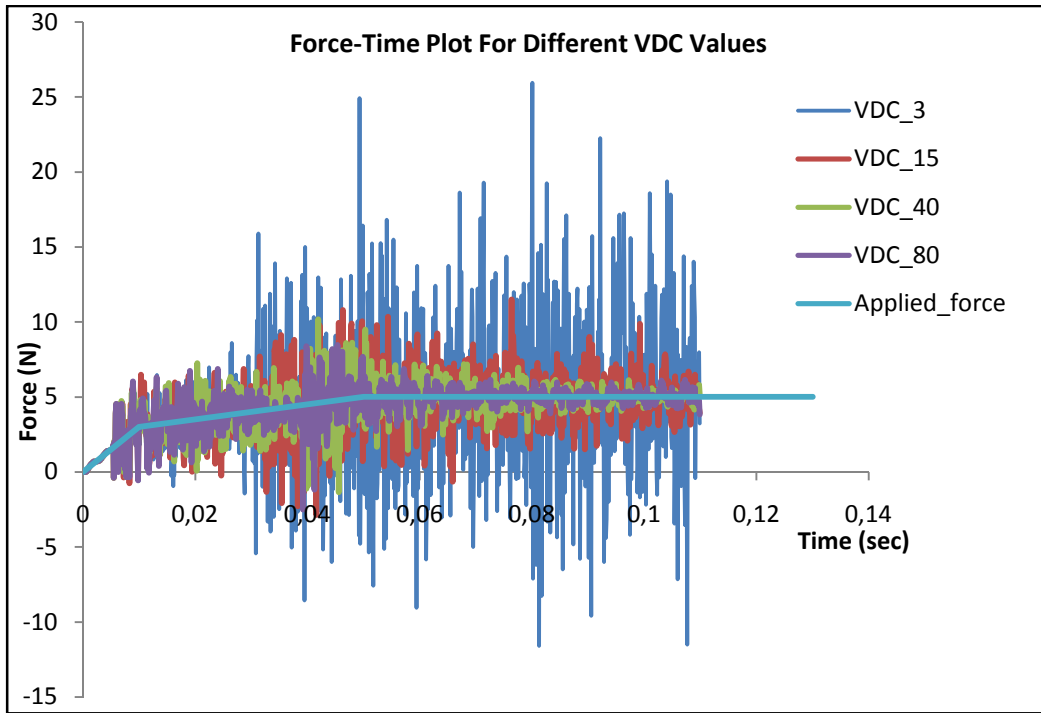
Figure 3.12. Effect of VDC Values On Total Force

As the physical structure is considered, there is contact and friction between the spring and the rod. Therefore, friction parameters should also be defined. In order to include the effect of contact, dynamic and static coefficients of frictions are input to the program. The program defines contact friction coefficient by using the following formula [21]:

$$\mu_c = FD + (FS - FD)e^{-DC \times Vrel} \tag{3.1}$$

where, μ_c is the coefficient of friction, FD is the dynamic coefficient of friction, FS is the static coefficient of friction, DC is the exponential decay coefficient, V_{rel} is the relative velocity between contacting parts.

In order to investigate the effect of friction, a shorter model is constructed for the helical spring in order to make runs in less amount of time. Properties of the simple spring are shown in Table 3.8 and physical structure is shown in Figure 3.13. Proposed short model also includes buckling of the spring and contact between the rod and spring.

32

Table 3.8. Properties of Shorter Spring

Property	Value
d(mm)	1.5
D(mm)	10
p(mm)	5
L_0(mm)	80
G(GPa)	76.9
Na	15.7
Material	AISI 1040
End-Condition	Plain-Plain
E(GPa)	200
υ	0.3
C(N/mm)	3.1
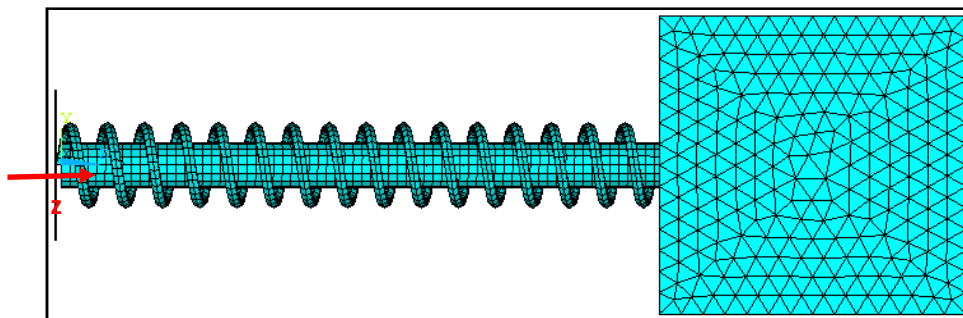
Figure 3.13. Shorter Model Structure

The friction coefficients are used as in reference [25] for the case of dry friction for hard steel on hard steel. The following parameters are used in analysis: FD= 0.42, FS= 0.78, DC=0.5 and VDC=20.

In order to investigate the effect of friction force, two models are constructed by using the model shown in Figure 3.13. The breech block hit the spring with 1500 mm/sec velocity. In one of the models, friction is defined by using the parameters shown above and the other model is constructed without defining any friction. Figure 3.14 shows the extracted reaction force values from the fixed nodes versus the displacement of the tip. As expected, presence of friction force between the rod and the spring decreases the amount of reaction force on the fixed nodes. In

order to investigate effect of friction deeply and extract friction forces, the guiding block is left free along the axis of the helical spring which is specified as z axis in Figure 3.13. The block is given an initial velocity of 1500 mm/sec's and made to compress the spring. In this model, one node is created and connected to the rigid rod in order to find the friction force between the rod and the spring. The node is fixed in all directions, hence friction force can be obtained as a reaction force from this node. Constructed model is basically shown in Figure 3.13 and a fixing node is created additionally as shown in Figure 3.15. Some sample runs are performed by changing certain parameters. Constructed models are shown in Table 3.9. Results of the analysis are shown in Figure 3.16 for the first three models.
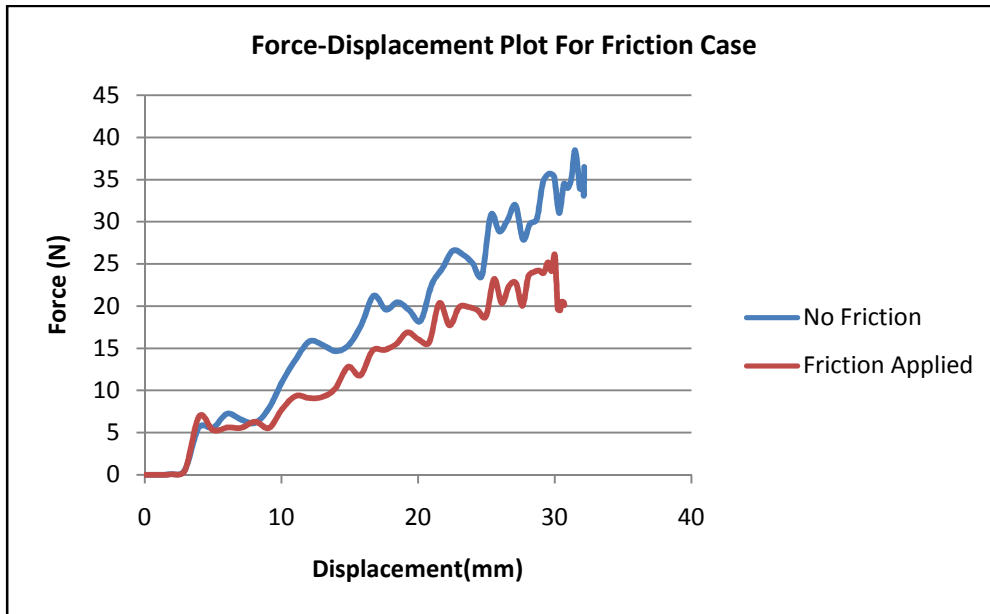

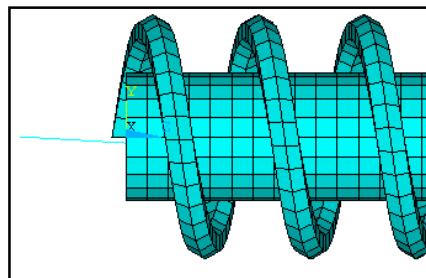**Figure 3.14.** Force- Displacement Plot For Friction Case

Figure 3.15. Rigid Element Between Rod and Fixing Node

Table 3.9. Parameters of Constructed Models

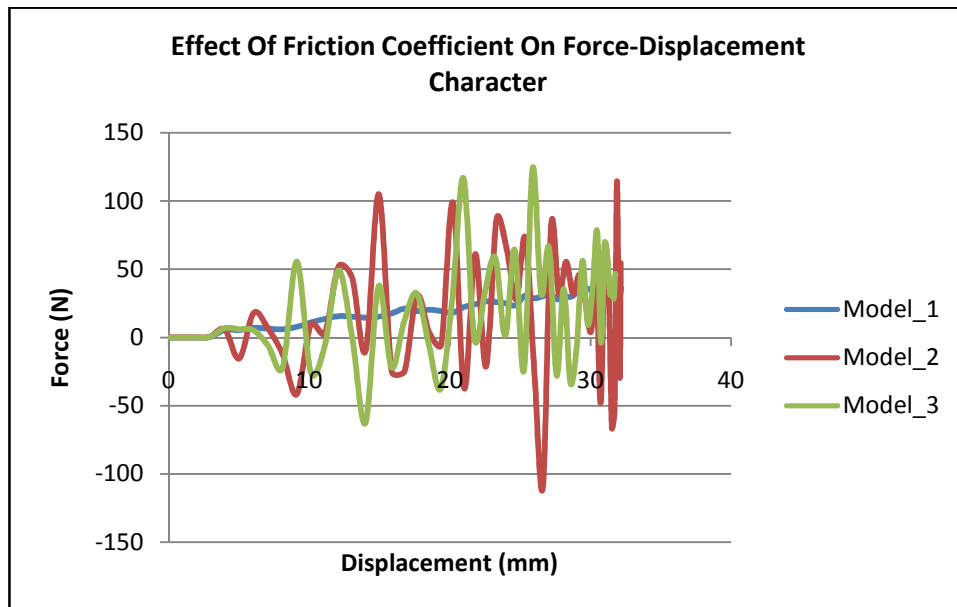| Model	Static Friction Coefficient (FS)	Dynamic Friction Coefficient (FD)	Decay Coefficient	VDC
1	-	-	-	-
2	0.1	0.1	0.5	0
3	0.78	0.42	0.5	0
4	0.78	0.42	0.5	20
5	0.78	0.42	0.5	40
6	0.78	0.42	0.5	60

Figure 3.16. Effect of Friction Coefficient on Force-Displacement Character

Figure 3.16 shows the total force transmitted to the rifle both from the helical spring and the rod versus the tip displacement of the spring. As expected, friction created a highly non linear and oscillating behavior on the force-deflection relation. Model 1 does not show non linear behavior when compared to the others. As friction increased (from going from Model 2 to Model 3), there has not been any increase in the friction force. The reason of this behavior may be the changing of normal force for Models 2 and 3 at the contacting surfaces. Comparison plot for Models 3, 4, 5 and 6 is shown in Figure 3.17. Figure 3.17 shows how force-displacement character is effected from VDC parameter change. As indicated in Table 3.9, VDC parameter increases going from Model 3 to Model 6. Force amplitudes are found by adding the total reaction forces obtained from the helical spring with the friction force obtained from the external node given in Figure 3.15. As Figure 3.17 is examined, it is seen that oscillatory behavior is the common point in all models. However, as VDC values increase, oscillations do not diminish. There is no specific

relation between the VDC parameter with the oscillatory behavior. Although VDC parameter increase from Model 4 to Model 6, oscillations do not die out. Model 3, which has zero VDC showed less oscillations when compared to others.
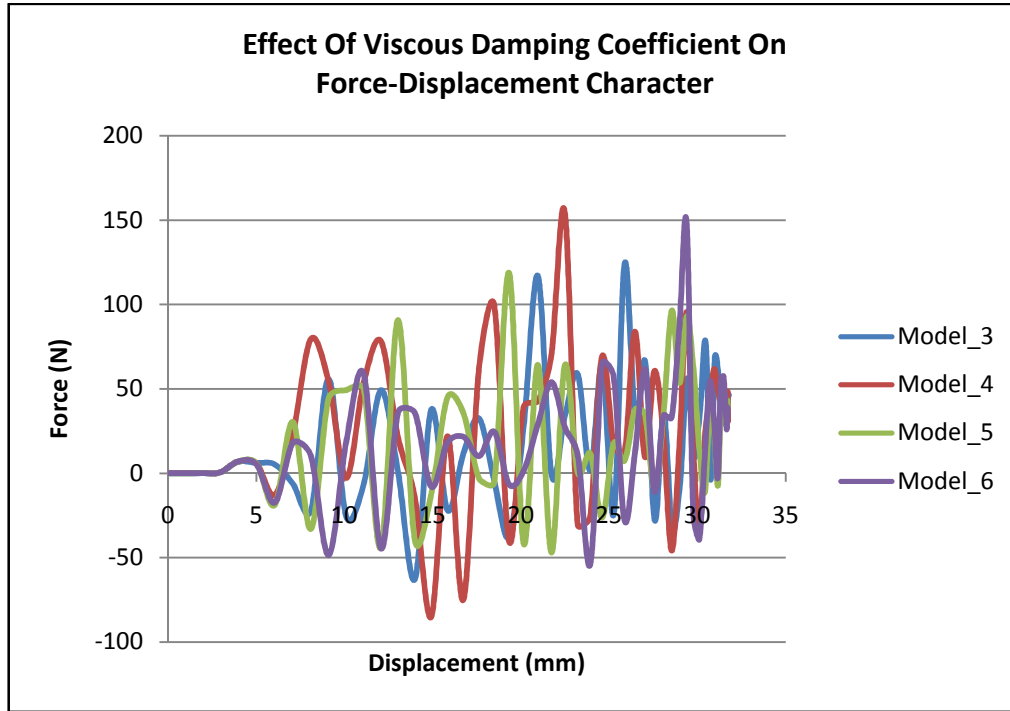

Figure 3.17. Viscous Damping Coefficient Effect On Force-Displacement Character

3.1.5 APPLIED LOADING CONDITION

As discussed in previous chapters, the process takes in a short period of time. Hence, velocity is high. For the Collision Model, the breech block is given an initial velocity of 1500 mm/sec. For the Simple Spring Model, the input can be either displacement or forcing which are functions of time.

3.1.6 DEFINING DAMPING IN THE MODEL

Damping is used to minimize the unrealistic oscillations in the response of the structure during transient analysis. Besides, applied damping should also reflect the physics of the structure. This section aims to give information about damping types in LS-DYNA and effects of damping on force-displacement character.

Both mass weighted (alpha) and stiffness weighted (beta) damping can be applied in LS-DYNA. Alpha and beta damping values are the damping factors in the below equation [24]:

$$[C] = \alpha[M] + \beta[K], \qquad (3.2)$$

where, α is Alpha damping (mass weighted), β is Beta damping (stiffness weighted), and

36

Rayleigh damping is used as in the following form [24]:

$$\xi_i = \frac{\alpha}{2\omega_i} + \frac{\beta\omega_i}{2} \ , \tag{3.3}$$

Modal damping, alpha and beta damping values are related with each other as shown in Equation 3.3. Modal damping indicates the Ith damping ratio and ω_i indicates the natural frequency of the Ith mode. It is advised to use the most dominant mode's natural frequency for finding the damping values.

In order to define the damping, there are three approaches. For a specified modal damping ratio, either alpha or beta is equated to zero and the remaining damping value is evaluated or, both alpha and beta can be specified. There are two frequencies, at which the amount of modal dampings are equal as shown in Figure 3.18. Then, two equations can be solved simultaneously to find the damping values.

$$\xi = \frac{\alpha}{2\omega_1} + \frac{\beta\omega_1}{2}, \tag{3.4}$$

$$\xi = \frac{\alpha}{2\omega_2} + \frac{\beta\omega_2}{2}, \tag{3.5}$$

In many structural problems, alpha damping (or mass damping) may be ignored (α=0). The modal damping can be evaluated by using Equation 3.6.

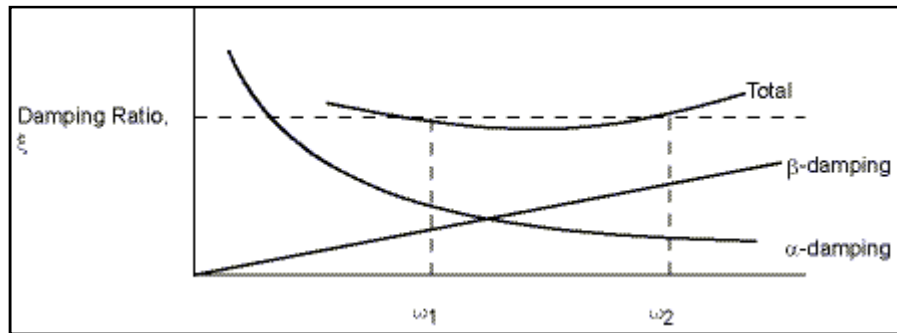$$\xi_i = \frac{\beta\omega_i}{2}, \tag{3.6}$$

Figure 3.18. Rayleigh Damping [24]

Mass proportional (alpha) damping is effective for low frequencies and will damp out rigid body motion. Stiffness proportional (beta) damping is effective for high frequency oscillations as can be understood from Equation 3.2.

Since every analysis in LS-DYNA takes hours to complete for the spring described in Table 3.1, a shorter spring model is constructed and sample runs are performed for different beta damping values in order to investigate the effect of damping on the force displacement character. Properties of the analyzed model is shown in Table 3.8. The breech block is given a velocity of 1500 mm/sec and different values of damping are applied to the spring. Figure 3.13 shows the structure of the overall model.

In order to set a proper damping value, the natural frequency of the first mode should be evaluated. For the complete system, it is found as 75 rad/sec by using the model in Figure 3.19. The node at the end of the spring is modeled as a point mass with the same mass of the block as in Figure 3.19 and it is connected to the spring with rigid elements. The spring is fixed from one end and the mass connected end is free to move along the axis of the spring. After finding the natural frequency, four models are constructed by using the alpha and beta values shown in Table 3.10.

Force displacement character for the compression phase of the spring is shown in Figure 3.20. As Figure 3.20 is observed, it is obvious that the change in damping ratio does not effect the force deflection characteristics of the spring. Models 1 through 3 use beta damping for the spring only, whereas in Model 4, damping is defined for all parts as alpha damping. Maximum displacement of the tip of the spring in Model 4 is less than the other three models.
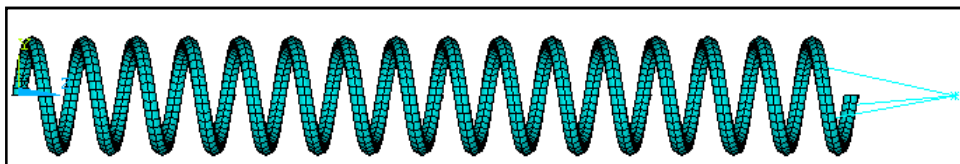

Figure 3.19. Model For Modal Analysis

Table 3.10. Applied Damping Values

Model	Damping Coefficient		Modal Damping for Corresponding Model
	Alpha	Beta	(Zeta)
1	0	6.58e-5	0.0025
2	0	6.58e-4	0.025
3	0	6.58e-3	0.25
4	15.2	0	0.025

It is seen that, damping values do not effect the force-deflection characteristics much. There is an oscillatory behavior in the stiffness character no matter what damping is applied. However, since there is material damping in the system, small amount of damping can still be applied. In a mechanical system like the recoil mechanism, the most dominant damping mechanism is the friction damping. By keeping in mind the necessary steps in modeling, a dynamic model is constructed in next chapter for the real recoil spring.
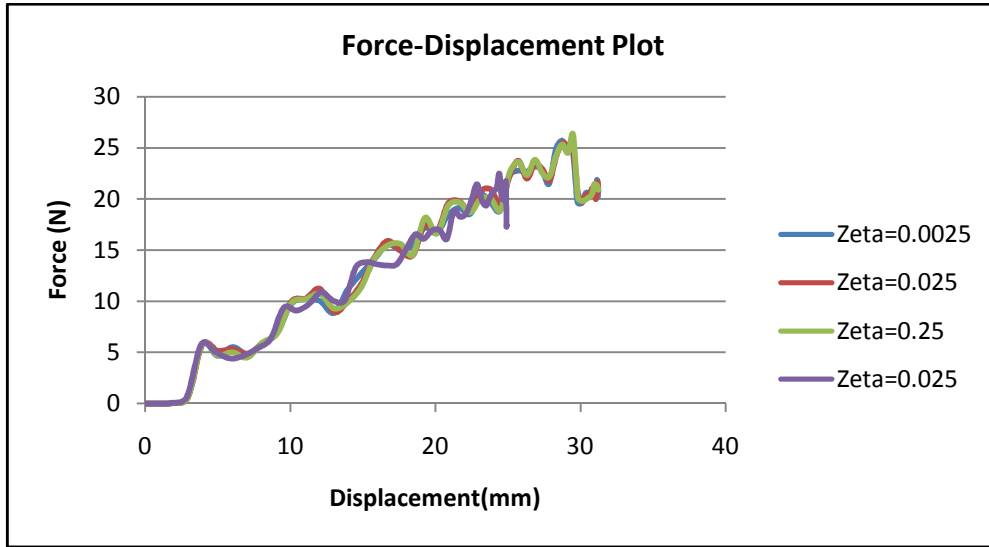
Figure 3.20. Damping Ratio Effect On Force-Displacement Character

3.2. FINITE ELEMENT MODEL CONSTRUCTION FOR THE RECOIL SPRING

In this section, finite element analysis is performed for the G3 recoil spring by using the knowledge gained from previous section. In order to see the results, three models are constructed for the recoil spring with the properties given in Table 3.1. Figure 3.21 shows the overall structure of the analyzed model.

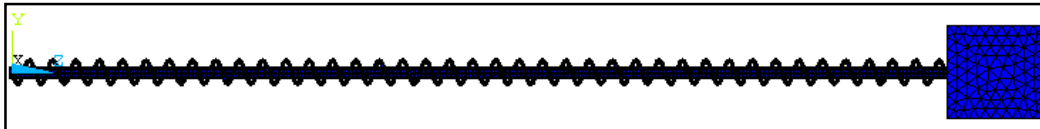**Figure 3.21.** Structure Of Dynamic Model

Three sample cases are analyzed for the real recoil spring. Table 3.11 shows the properties of the analyzed models. Like in previous cases, the breech block is given an initial velocity of 1500 mm/sec and made to hit the spring.

Table 3.11. Recoil Spring Model Properties

MODEL	1	2	3
Damping Ratio (zeta)	0.02	0	0

Table 3.11 (cont'd)

FS	0	0.78	0.78
FD	0	0.4	0.4
VDC	0	0	20

Deformed shape of the models are all like in Figure 3.22, exhibiting a "s" form which indicates presence of buckling. Figures from 3.23 to 3.25 depicts the force-deflection characteristics for the three cases. As Table 3.11 is examined, it is seen that Model 1 has some amount of damping only. Model 2 has only friction and Model 3 has friction and some amount of viscous damping for contact. Friction force in Models 2 and 3 are extracted by using the method described in Figure 3.15. An additional fixed node is connected to the guiding rod in order to prevent its movement along the compression axis of the spring and reaction force in z direction is extracted from this fixed node. Three nodes are selected from the end turn of the recoil spring as explained in Section 3.1.3.

Figure 3.23 shows the results obtained for damping ratio of 0.02. Since there is contact between rod and spring, the behavior has oscillations. Figure 3.24 shows the results obtained for Model 2. When compared to previous model, it is obvious that total force amplitudes increased. The friction force is present for Model 2 and that is why force amplitudes increased. Model 3 includes the effect of VDC parameter as well with the same amount of friction coefficients as in Model 2. Figure 3.25 shows the force displacement relation in third model.
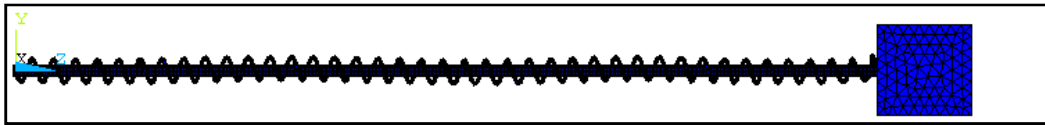

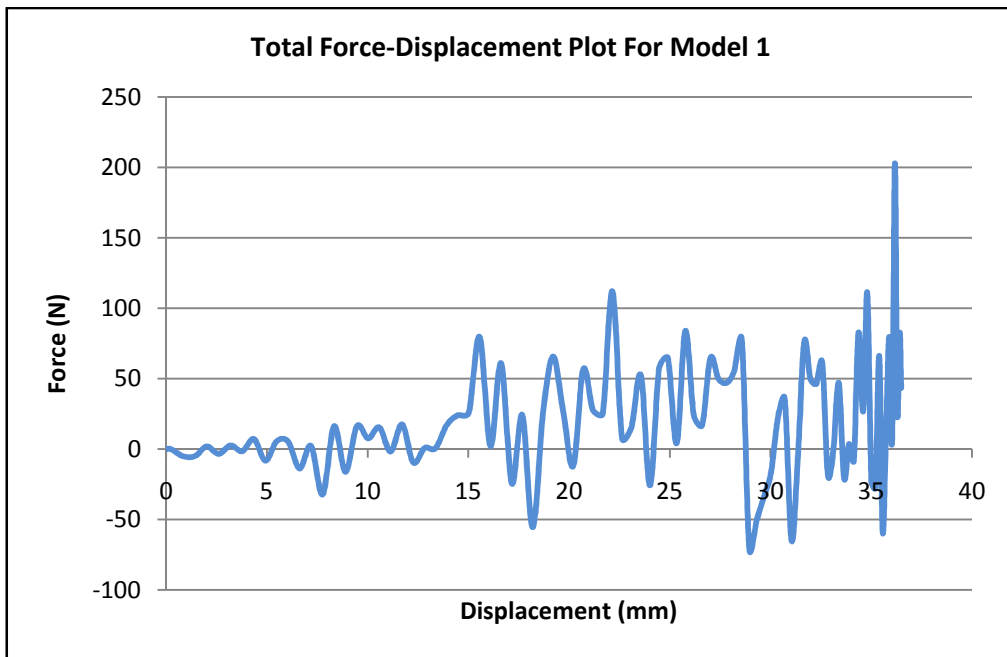**Figure 3.22.** Deformed Shape of the Recoil Spring

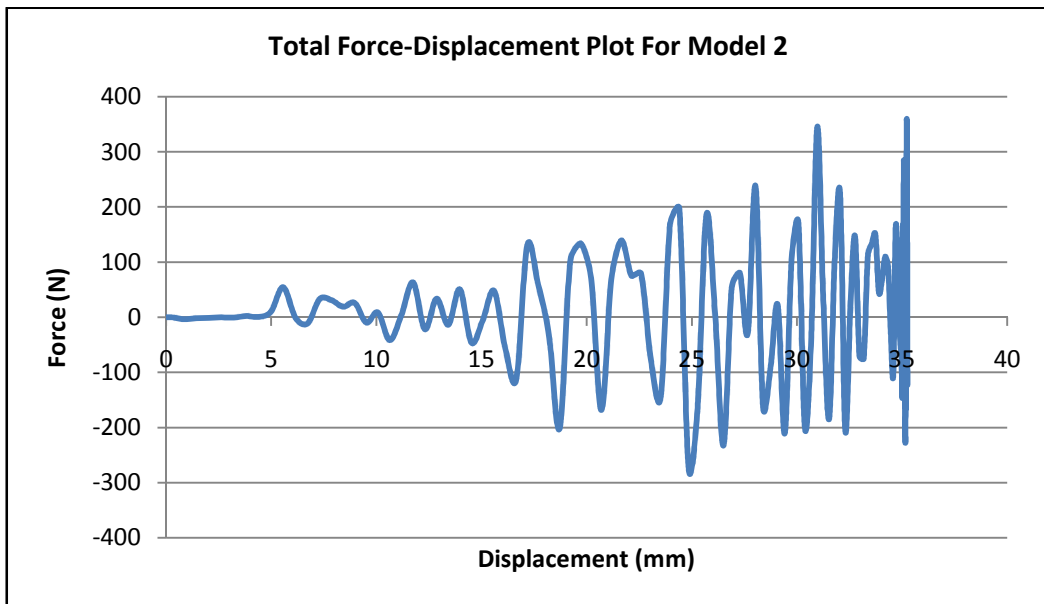**Figure 3.23.** Total Force Displacement Plot for Model 1

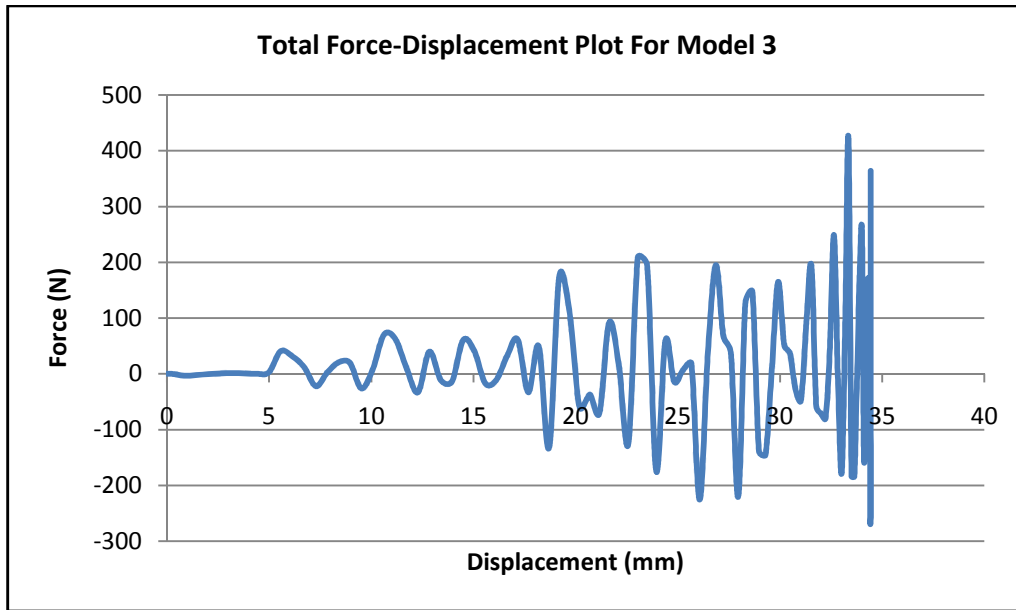**Figure 3.24.** Total Force-Displacement Plot for Model 2

Figure 3.25. Total Force-Displacement Plot For Model 3

At first glance on Figure 3.25, the maximum displacement decreased when compared to Model 2 which is expected because VDC parameter is not zero. Although there are small amplitude differences in total force reaction, Models 2 and 3 are close to each other. VDC parameter decreased the amount of total deformation slightly.

Finite element models can also give amount of stresses at any point at any time or deformation. Figure 3.26 shows the maximum Von Mises Stress at maximum deformation. Figures from 3.26 to 3.28 show the von Mises Stress outputs for the models. When these plots are observed, maximum stress amplitudes occur at the contact point of spring tip with the breech block. In order to make a comparison between models, one node is selected and von Mises and shear stresses at this node is compared in Table 3.12. Node 9500 is selected for comparison which is located on the YZ plane at the beginning of the third coil from free end. When Table 3.12 is observed, both shear stress and von Mises stress outputs are close for the three models. Hence, parameter differences between models do not affect the stress outputs significantly.
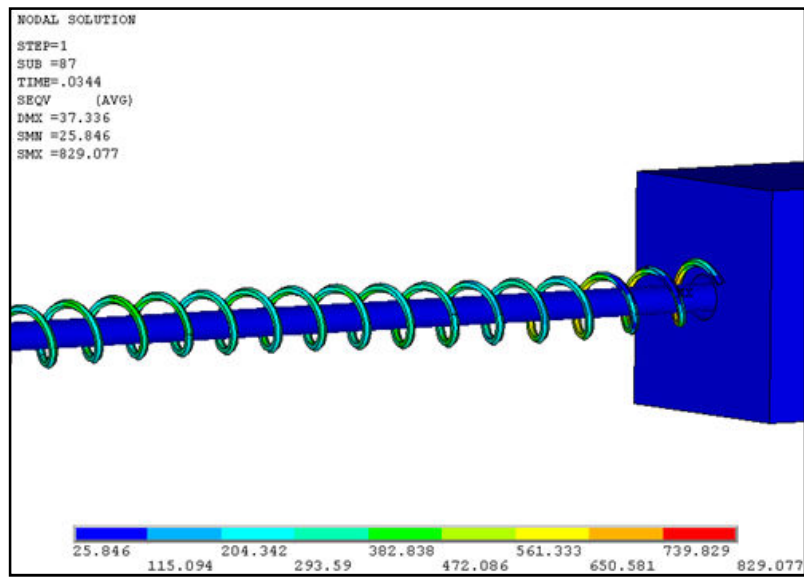
Figure 3.26. Von Mises Stress Distribution For Model 1
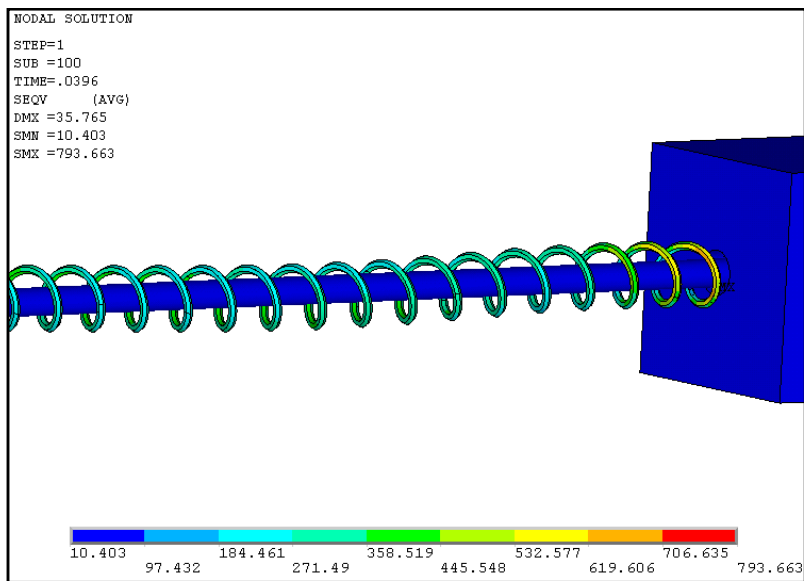
Figure 3.27. Von Mises Stress Distribution For Model 2

```
NODAL SOLUTION

STEP=1
SUB =102
TIME=.04
SEQV    (AVG)
DMX =34.271
SMN =8.276
SMX =750.361
```

```
8.276        173.184      338.091        502.999       667.907
      90.73        255.637      420.545        585.453       750.361
```

Figure 3.28. Von Mises Stress Distribution For Model 3

Table 3.12. Stress Output Comparison For Selected Node For Each Model

Stress Outputs From	MODEL		
Node 9500	1	2	3
YZ Shear (MPa)	124	120	130.5
Von Mises (MPa)	269	251	260

44

CHAPTER 4

VERIFICATION TEST

In the previous chapter, finite element modeling methodology is studied in detail. In this chapter an actual helical spring is tested so that it can be used to validate the developed modeling and analysis methodology. Detailed information about the experimental set up and experiment is also given in this chapter.
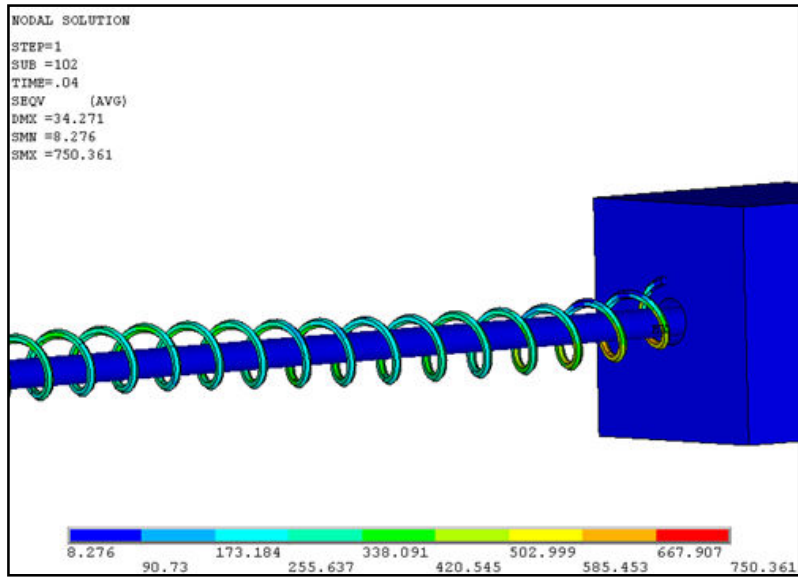
Although the impact velocity in actual operational conditions of recoil spring is high, in ideal case, the experiments on a representative recoil spring needs to be done with high velocity cameras and set up. But in our case, there are limitations to the available equipment to conduct the experimental work on helical springs. Main limitation is the maximum velocity that can be reached with test system. Another limitation is the minimum available size of the strain gage that will be bonded on the spring to be tested. Unfortunately the strain gage is too large for the G3 recoil spring which has a wire diameter around 1.5 millimeters. Because of these limitations a spring with a larger wire diameter is used and the test is conducted at a relatively low speed. Details are explained in the following sections.

4.1. LARGE WIRE DIAMETER SPRING DEFINITION

For the stress measurements to be made, a strain gage should be bonded to the point of interest. For a G3 recoil spring, this is impossible since the wire diameters are small around 1.5 mm. There is no such small strain gage available commercially. Hence, it is required to define a helical spring and deformation so that there would be no permanent deformation on the spring and the stress outputs can easily be monitored by bonding a strain gage on the specimen. Besides, the buckling behavior should also be seen in the new spring which is used in the experiment. In order to observe the effect of buckling, the spring deformation should be larger than the critical deflection amount.

The helical spring configuration to be used in the experiments is defined in Table 4.1. The maximum allowable shear stress is given as 800 MPa for this material. Therefore, without any plastic deformation, the spring can be compressed for 60 mm's. For this deformation, buckling behavior will also be seen.

Table 4.1. Properties of Helical Spring in Analysis and Experiment

Property	Value
d(mm)	5.2
D(mm)	35
p(mm)	20
L_0(mm)	405
G(GPa)	80

Table 4.1 (cont'd)

Na	40
Material	17223 Class D
End-Condition	Plain-Plain
E(GPa)	208.5
C(N/mm)	8.53
Buckling Deformation (mm)	35
Allowable Shear Stress (MPa)	800
Applied Maximum Compression (mm)	60
Shear Stress At Maximum Compression (Mpa)	392

4.2. PHYSICAL STRUCTURE OF TEST SET UP

The test is performed in materials laboratory of the Middle East Technical University Mechanical Engineering Department by using a tension-compression test machine. The compression machine is manufactured by Zwick Roell and it is capable of applying 4 KN force in both compression and tension. Since the software shows the amount of deflection and the load cell shows the amount of force applied, it is easy to find the force deflection characteristics. Stress outputs are collected from the stain gages. Figure 4.2 shows this test machine. However, this machine is not sufficient for dynamic applications where the compression rate is high. Hence the spring is compressed with the maximum speed that the machine can supply, which is 1000 millimeter/minute.

Figure 4.1, shows the experimental set up. The spring seat has three elevated points inside, in order to touch and constrain the spring from three points. This is the same boundary conditions used in the finite element method. However, as the assembly is set, it is seen that the seat part advances towards the spring. This effect diminishes when there is an applied load on the spring. Hence in order to adjust preliminary settings such as displacement and mounting, it is a necessity to locate the spring by using some amount of adhesive. For this purpose, an elastic adhesive is applied. See Figure 4.3 for application of adhesive on the spring seat.
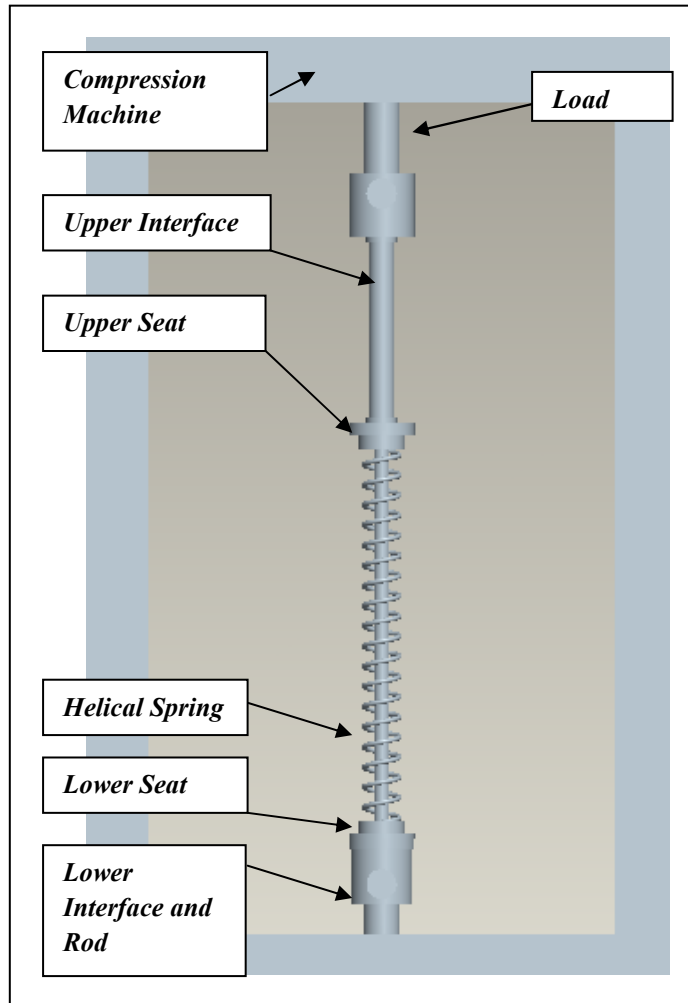
Figure 4.1. Compression Test Structure

Figure 4.2. Zwick Roelle Test Machine

Adhesive

Spring Seat

Helical Spring

Figure 4.3. Application of Elastic Adhesive Between Seat and Spring

48

In order to determine the stresses in the spring, strain gage rosettes are bonded to the spring. Locations of the rosettes are determined randomly. Four, rosette type gages are bonded at equal angles to cover one coil of the spring. The selected coil is in the seventh turn from the application point of displacement. Gages are bonded to the inner surfaces. Gages are located in a way that, two of them are aligned with the plane which passes through the end turn start. Remaining pair is bonded with an angle of 90 degrees to this plane. Larger number of gages were bonded in order to have spare gages to be used when necessary. Figure 4.4 shows the application points:
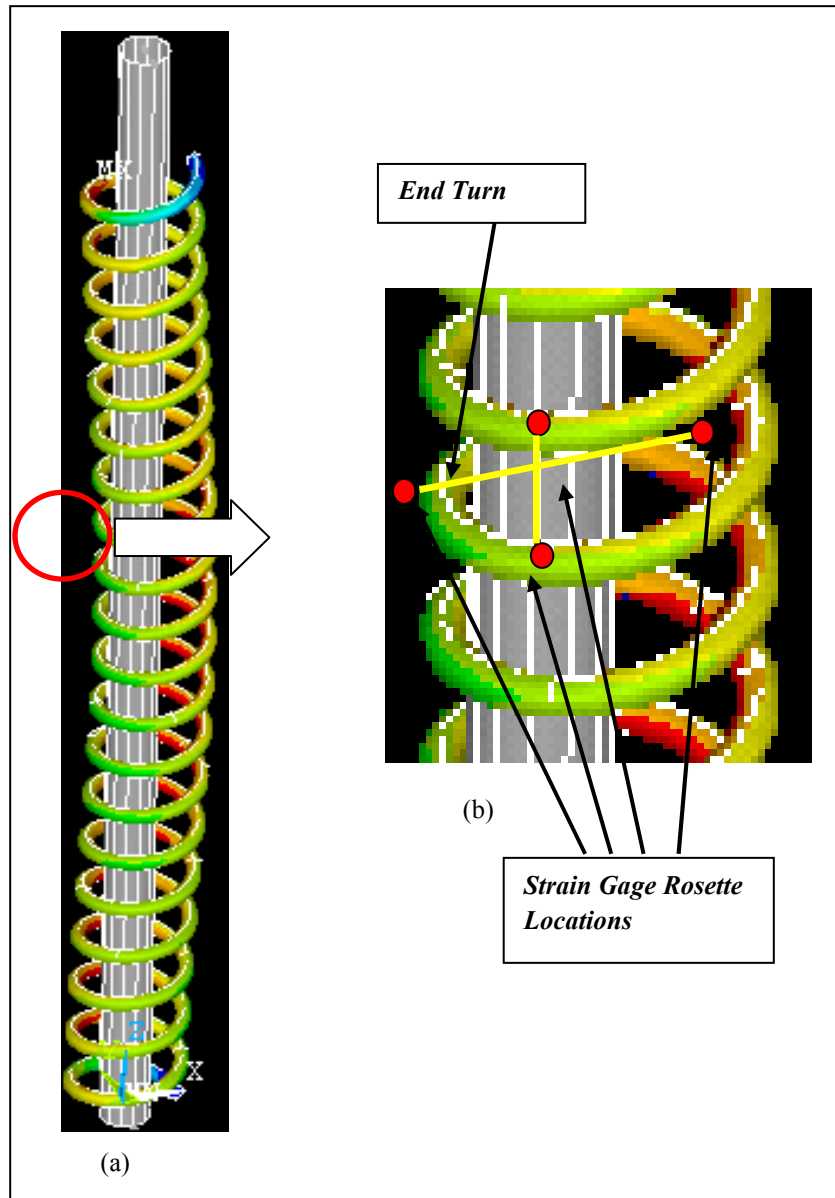

Figure 4.4. a) Deformed Spring b)Detailed View of Gage Locations

Before applying the strain gages, the surface of the steel spring has to be cleaned from rust, paint, grease or any kind of contaminant. For this purpose, the surface of the material is polished with a #120 abrasive paper. Then, in order to remove fine dust, acetone is used to clean the bonding surfaces. Next, the special bonding adhesive is applied to the backside of the gage and then pressed against the spring surface. Figure 4.5 is taken just after the bonding process.

Next, the lead wires are soldered to the terminals in order to relieve stress in the lead wires. Then those terminals are connected to the quarter Wheatstone bridge. Figure 4.6 shows the terminals and the connections. The number of strain gages are selected as four by considering the possible defects induced in the strain gages during bonding or soldering. Besides, since there will be buckling, there is a risk of strain gage rubbing to the guiding rod. It is better to keep spare gages on the specimen in case there is rubbing.

Figure 4.5. Strain Gage Close View

Figure 4.6. Solder Terminals

After installation of the spring into the assembly, the strain gages are connected to the Wheatstone cable bridge. Quarter bridge Wheatstone circuit is used. Strain gage terminals are connected to the data acquisition system. Then gages are calibrated by using the software inside the set up and the bridge cables. For temperature compensation, no action is taken since the temperature inside the laboratory is stable and same during bonding the strain gages and experiment. The strain gage rosettes are the smallest available in the market, which has backing material of Ø5 millimeters and the gage diameter is Ø1 millimeter. Gages are manufactured by TML and their type are FRA-1-17.

The data acquisition system is capable of acquiring data with high frequency. During the experiment, data is extracted with sampling frequency of 2000 Hz in order to see possible oscillatory behavior that is seen in finite element models.

During experiment, the input voltage is selected as 5V since the resistance of the gage is 120 Ω. If higher voltage is applied, then the temperature rise in the gage will be higher and the amount of temperature output would be higher. Generally, higher voltages are applied to the higher resistances such as 350 Ω or larger. Figure 4.7 shows the entire set up, which is ready to perform the experiment.

Figure 4.7. Test Set Up

4.3. TEST PROCEDURE

After locating the mechanical structure, strain gages are calibrated according to the instructions given in the data acquisition system. After calibration, the spring is compressed with a velocity of 1000 mm/min up to 60 millimeters of deflection and stopped for 5 seconds, then decompressed. During compression, all required data are collected such as voltage change in the bridge and force-deflection output from the Zwick test machine.

4.4. TEST RESULTS

Figure 4.8 shows the voltage output from the strain gage. The linear stiffness of the spring is found to be 8.2 N/mm by compression test. Analytical results imply 8.5 N/mm as indicated in Table 4.1. The small difference may be originated because of the small difference between the modulus of elasticity of the spring material and the value used in calculation. Besides, end condition in reality may have caused this small difference. Deformed shapes and shear stress outputs from the gages are given in Table 4.2. Spring compression is shown in Figure 4.9.

The spring is compressed up to 60 millimeters and intermediate steps are photographed in order to observe buckling behavior. As previously mentioned in Table 4.1, the critical deformation for buckling is found as 35 millimeters. When Table 4.2 is examined, buckling occurs before 40 millimeters of compression which confirms analytical calculations. Around 20 millimeters of deformation, no buckling is observed. Gage shear stress outputs are evaluated by using Equations A2 to A4 in Appendix A. One sample calculation is shown in Appendix B.

Figure 4.11 shows the maximum shear stress distribution from the gage location throughout the experiment. There are small oscillations when compression reaches maximum value. However, those are not significant. Besides, around 3 seconds, the plot changes its constant slope and shows a small shift. This instant corresponds to the point at which buckling occurs. This instant corresponds to 33 millimeters of deformation.
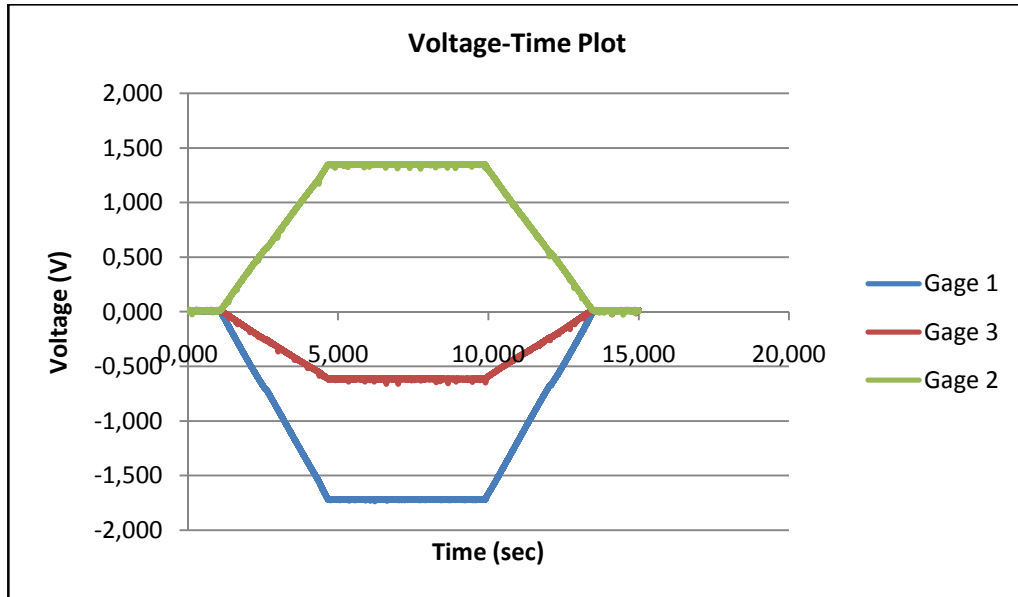

Figure 4.8. Voltage Output From Strain Gages With 2000 Hz Sampling Frequency
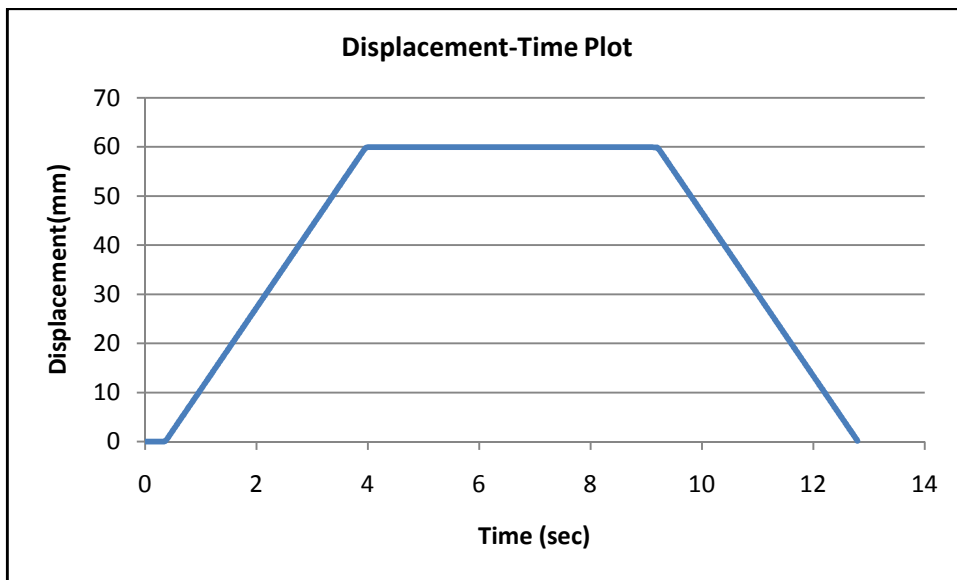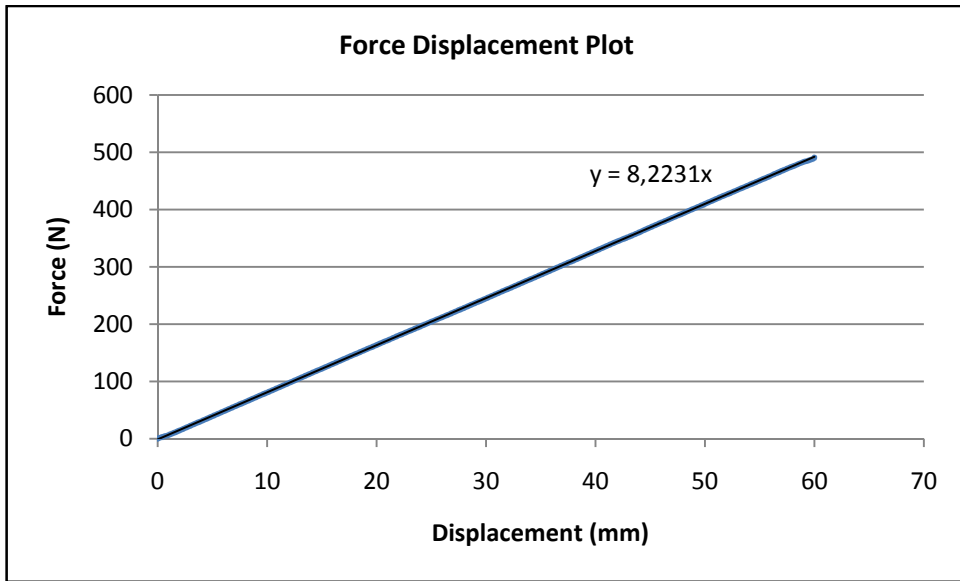

Figure 4.9. Displacement-Time Plot

Figure 4.10. Force-Displacement Plot For Compression

Table 4.2. Deformed Shapes And Gage Outputs

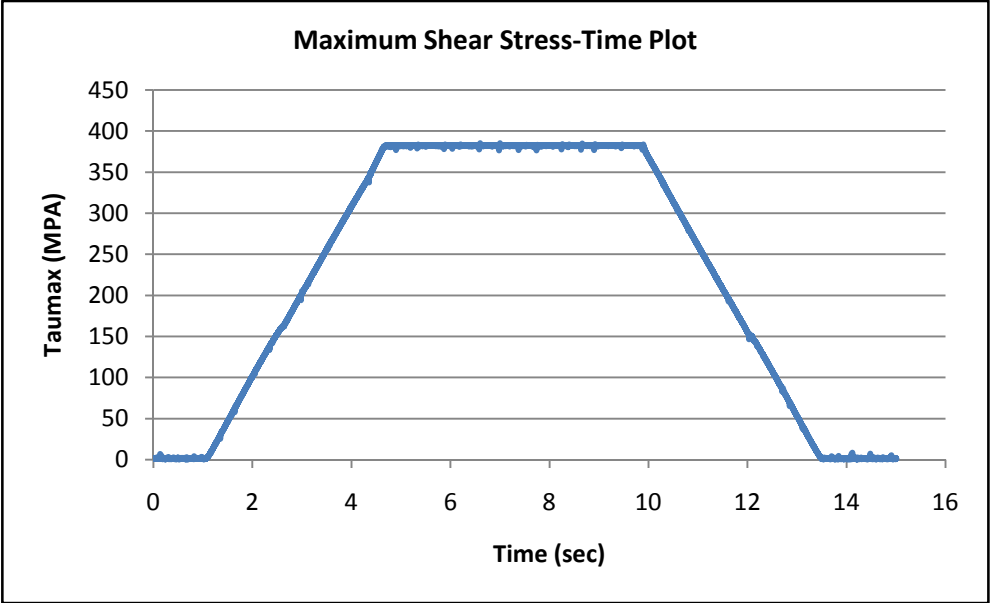| Compression Amount	20 millimeters	40 millimeters	60 millimeters
Deformed Shapes			
Gage Shear Stress Output (MPa)	127	251	314

54

Figure 4.11. Maximum Shear Stress Output From Gage Location Versus Time Plot

CHAPTER 5

FINITE ELEMENT MODEL CONSTRUCTION

In Chapter 4, compression test is applied on a helical spring in order to find stress and force deflection characteristics. This chapter aims to create a finite element model of the same spring tested which is defined in Table 4.1. In order to construct the finite element model of the spring, modeling approach defined in Chapter 3 is applied step by step. As discussed in previous section, the spring is compressed in the test machine. Therefore, the boundary condition is used as displacement. For this purpose, a Simple Spring Model is used in the models.

5.1. MESHING

Meshing is performed with SOLID 164 elements with edge length of 4 mm. The edge length effect is discussed in section 5.3. Before making an analysis, it is necessary to make a sensitivity analysis on the edge length parameter. The guiding rod is meshed with rigid elements as explained previously.

5.2. APPLIED BOUNDARY CONDITION

As mentioned before, three nodes from two ends are selected for application points of the boundary conditions. Figure 5.1 shows the application points of the fixed nodes. The spring is compressed with the actual compression speed of the test set up, which is 1000 mm/min.

The model in Figure 5.1 is meshed with edge length of 4 mm. There are 27 segments in one turn of the coil. Hence each segment corresponds to 13 degrees. Consequently, the angle between nodes 843 and 851 is 50 degrees. It is important to adjust 50 degrees between those nodes since the experimental set up touches the spring with the same angle from the elevated points. Same approach is used for the upper turn at which displacement input is applied. Figure 5.2 shows the application. This three node approach is also used in dynamic model construction. Table 5.1 shows the applied boundary conditions on the selected nodes. Boundary conditions are applied as displacement inputs as a function of time. The compression head velocity is known since it is set by the user in the laboratory. The moving nodes are given the input that is shown in Table 5.1. Although, in reality, the displacement in the recoil mechanism is so fast, applied data is limited to the capacity of the test machine.
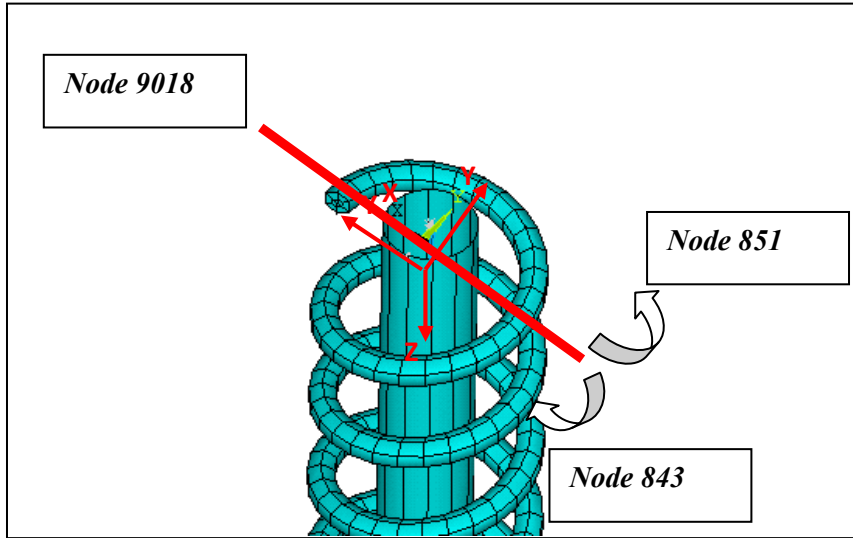
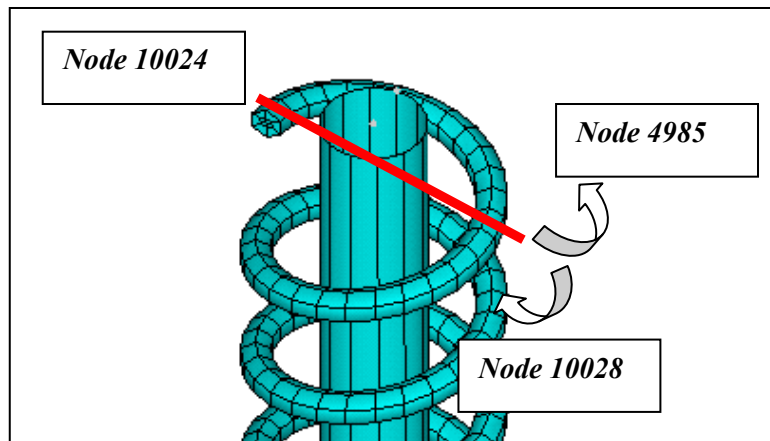**Figure 5.1.** Node Selection For Boundary Condition Application- Fixed Boundary

Figure 5.2. Node Selection For Boundary Condition Application- Displacement Input

Table 5.1. Applied Boundary Conditions On Selected Nodes

Displacement (mm)	Time (sec)
0	0
-30	1.8
-60	3.6

5.3. EDGE LENGTH EFFECT ON ACCURACY

As mentioned before, it is necessary to set a proper edge length while meshing the spring. In order to investigate the effect of edge length, the analysis should be performed three or more times with different edge lengths by using simple and fast static analysis. The results should settle around a value. As a result, the finite element model converges to a value and becomes insensitive to edge length effects.

For this purpose, the spring is meshed with three different mesh sizes for a simple static analysis. The edge lengths used are 3 mm, 4 mm and 4.5 mm. Then stiffness and stress results are compared for those models. Stress output is obtained for a node at or near a certain coordinate position. Since edge lengths are different, it is impossible to locate a node at the same position each time. Therefore, one coordinate is selected for stress results.

To start with, the analysis is performed for a model with edge length of 3. Figure 5.3 shows the model. There are 39 segments per coil. In reference [9], the segment per coil is advised to be 20. Higher number of segments implies more elements and nodes. Hence, solution time increases. For the next iteration, edge length of 4 mm is utilized. Figure 5.4 shows the analyzed model. In this model, since edge length increase, the number of segments per coil is counted as 28. This time it is close to the recommended number as in reference [9]. Finally, model with an edge length of 4.5 mm is constructed. This model is shown in Figure 5.5. As this model is investigated, the number of segments is found to be 27 per coil. Although, this number confirms with previous model, the wire cross section is no more a circle, instead it is in square form. This shape change can cause accuracy problems for the analysis.
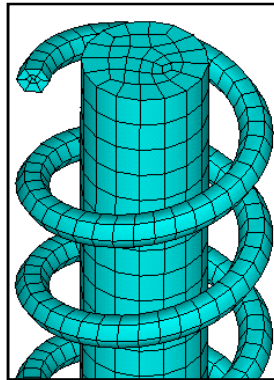

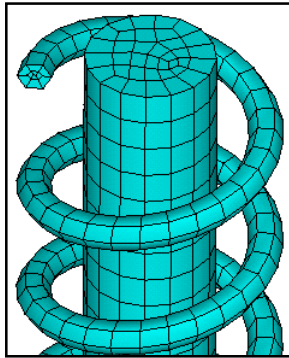**Figure 5.3.** FE Model With Edge Length: 3

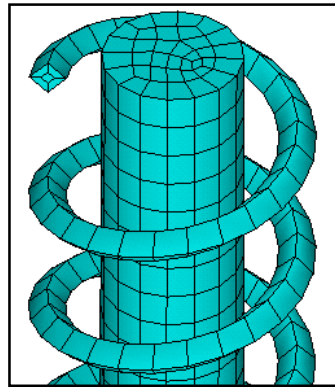**Figure. 5.4.** FE Model With Edge Length: 4

Figure. 5.5. FE Model With Edge Length: 4.5

For result comparison, a node is selected in the model and position coordinates are recorded. For the rest of the models, other nodes at or near those coordinates are searched for. Result comparison is shown in Table 5.2. Since given displacement boundary condition is known, it is straightforward to find the stiffness. As shown in Figure 5.1, three nodes are selected as fixed nodes. By using the finite element model, axial force reactions can be found. The ratio of total axial force to final deflection value leads to the stiffness. As Table 5.2 is observed, it can be stated that stiffness results are close for three of the models. However, stress results deviate slightly for the third model. This difference originate due to shape change of the cross section from circle to square. As the result trends are observed, it can be stated that using edge length of 4 mm gives almost the same results with the model constructed by using an edge length of 3 mm. Hence, it is a wiser choice to use edge length of 4 mm in order to get accurate results without increasing analysis time.

Table 5.2. Comparison of Results For Different Edge Length

Property	MODELS		
	Edge Length: 3mm	Edge Length: 4mm	Edge Length: 4.5mm
Deformation (mm)	60	60	60
Total Reaction Force (N)	495	495.3	483.3
Stiffness (N/mm)	8.25	8.25	8.05
Segments per Coil	39	28	27
Node Number of Interest	3635	2677	1545
Total Node Number	39003	28600	14694
Von Mises Stress (MPa)	769.13	770	827

5.4. CONSTRUCTED MODELS AND RESULTS

In order to see effect of friction and damping, three models are constructed and the most accurate result (the one with the best agreement with analysis results) is sought for. Since experiment is performed, parameters are modified in order to make the finite element analysis results close to experimental results.

Stress results are collected from nodes which correspond to the actual gage position on the helical spring. Figure 5.6. shows the nodes from which results are extracted. Those results are the YZ shear stress component. Average of those outputs are calculated. First model is constructed as explained in section 3.1.3. In order to find friction force, one node is created under the rod and fixed in all directions. Then a rigid link is connected created between the rod and this node. Friction force data is collected from this node. Summation of this force output with the ones obtained from the tip of the spring gives the total transmitted force.
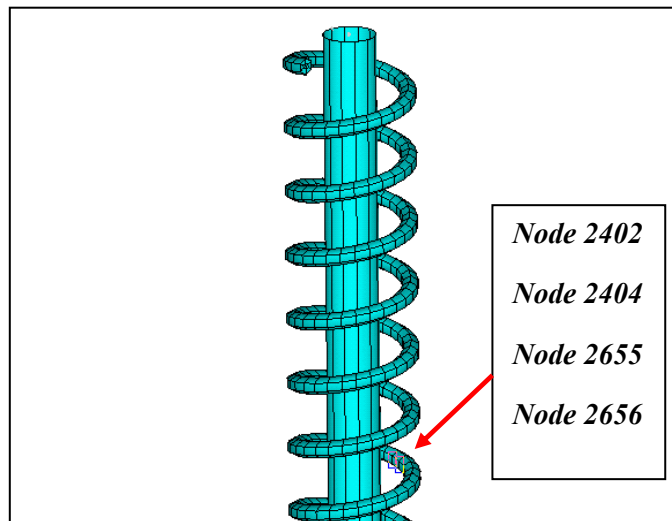
Figure 5.6. Position of the Stress Output Nodes

5.4.1 CONSTRUCTION OF MODEL 1 AND RESULT EVALUATION

This model includes the effect of friction only. For this model, parameters used are FS=0.78, FD=0.42, and VDC=0. Figure 5.7 shows the total reaction force obtained from the fixed nodes versus the deformation. When the deformed shape of the analysis is examined, it is seen that the oscillatory region between 30 mm to 40 mm of deformation correspond to the time at which the spring touches the guiding rod. In Figure 5.7, as amount of deformation increase, oscillations start in the force deflection curve. The reason for this behavior is the contact between the rod and spring inner surface. However, in the experimental results there are no oscillations. The reason of this may be mistuned parameters. Two more models are to be constructed to approach experimental results.

Between deformations of 15 mm and 20 mm, there is a change in slope in Figure 5.7. The reason might be mistuned parameters since this behavior is unexpected. Besides, it is not observed in experimental results. Figure 5.8 shows the average shear stress from four nodes versus displacement. When Figure 5.8 is examined, it is seen that the amplitude and behavior of the shear stress component does not conform with the experimental results. Significant drop of shear component at displacement of 15 mm is unexpected. The reason may be mistuned parameters or the YZ shear component does not coincide with the principal direction of the maximum shear stress in the experiment. Besides, the complete pattern is different from Figure 4.11.

Similar to Figure 5.7, there is an unexpected drop in shear stress between deformations of 15 mm and 20 mm in Figure 5.8. This drop coincides with the drop in Figure 5.7. Again, this behavior is unexpected since, as the spring is deformed, shear stress is expected to have an increasing pattern.
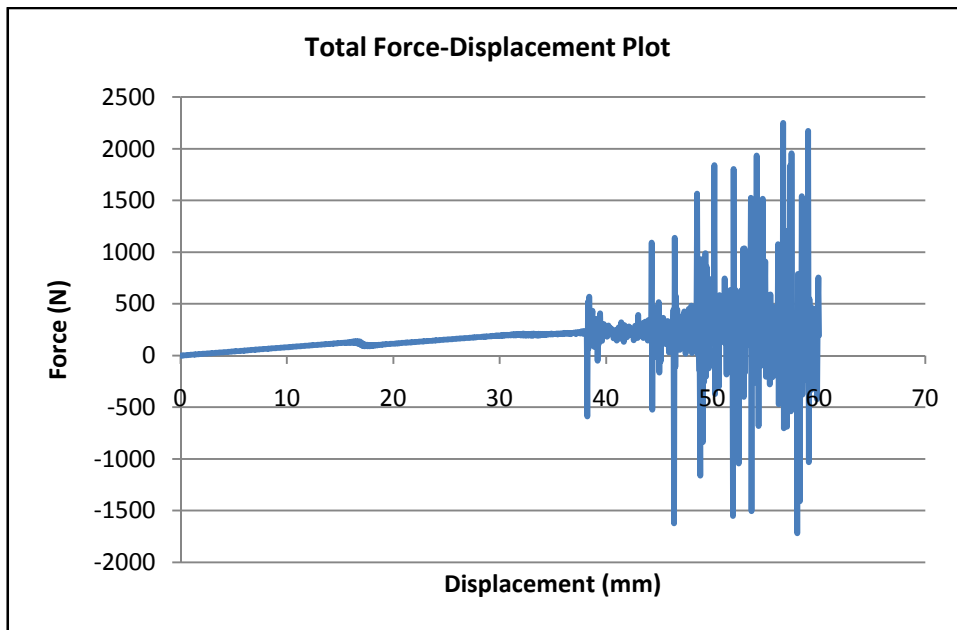
62

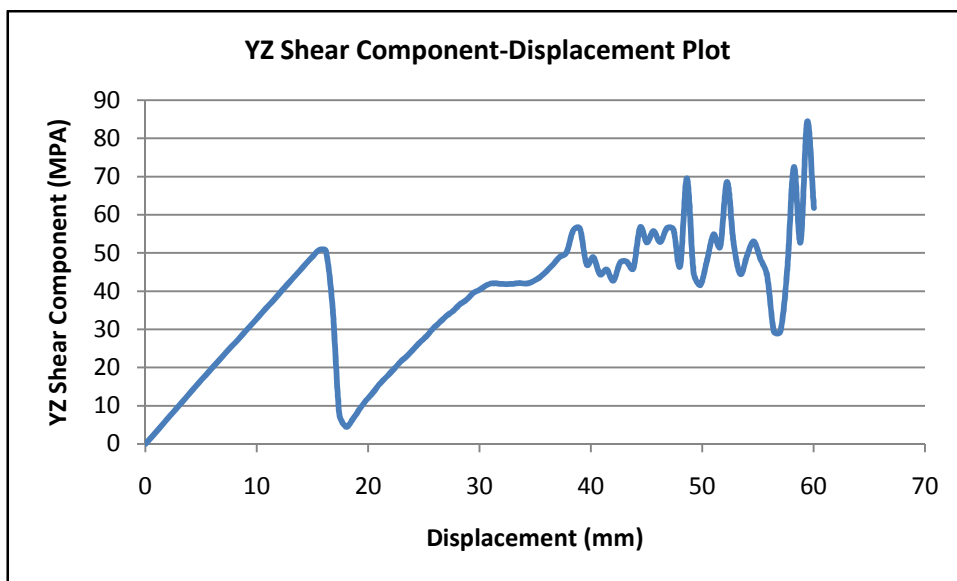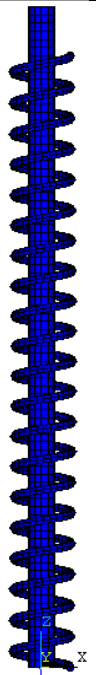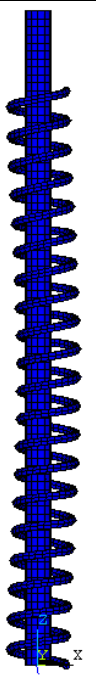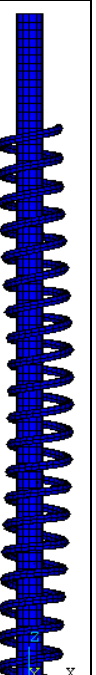**Figure 5.7.** Total Force Displacement Plot For Model 1

Figure 5.8. YZ Component of Stress-Average of 4 Nodes

Deformed shape of the spring for compressions of 20,40 and 60 millimeters and corresponding shear stresses are shown in Table 5.3. Table 5.3 also shows the YZ shear stress output from the finite element model and compares them with the results obtained by analytical methods and experiment. It is obvious that, analytical and experimental results show good conformity. However, shear stress amplitudes are far away from the experimental and analytical results.

63

The reason for this may be mistuned parameters during analysis. Hence, it is important to set the parameters accurately.

For the deformed shape, it is seen that they are close to the experimental results as shown in Table 4.3. Buckling behavior is seen as expected by the analytical results in 40 millimeters of deformation. A second model, Model 2, is constructed in next section to improve agreement between analysis and experimental results.

Table 5.3. Model 1 Deformed Shape and Stress Output Comparison

Compression (mm)	20	40	60
Deformed Shape			
YZ Shear Stress-FEA-Average (MPa)	13	49	61
Analytical Shear Stress (MPa)	130	261	392
Experimental Shear Stress Results (MPa)	132	253	382

5.4.2 CONSTRUCTION OF MODEL 2 AND RESULT EVALUATION

For Model 2, the same friction parameter is kept as in Model 1 with an additional VDC parameter in order to decrease oscillations after contact occur between rod and ring inner surface. Parameters of this model used are FS=0.78, FD=0.42, And VDC=20. Force displacement curve for this model is plotted in Figure 5.9. As Figure 5.9 is observed, it is seen that starting from 38 millimeters of compression, the character shows an oscillatory behavior. The reason for this is the contact between rod and spring. However, the magnitude of oscillations are small when compared to first model. VDC parameter decreased the amount of oscillations in the force displacement character for the region where there is contact between the rod and the spring.

There is a sudden decrease in the slope for deformations between 15 and 20. The reason for this unexpected behavior may be mistuned parameters. Figure 5.10 shows the average YZ shear stress obtained from the finite element analysis.
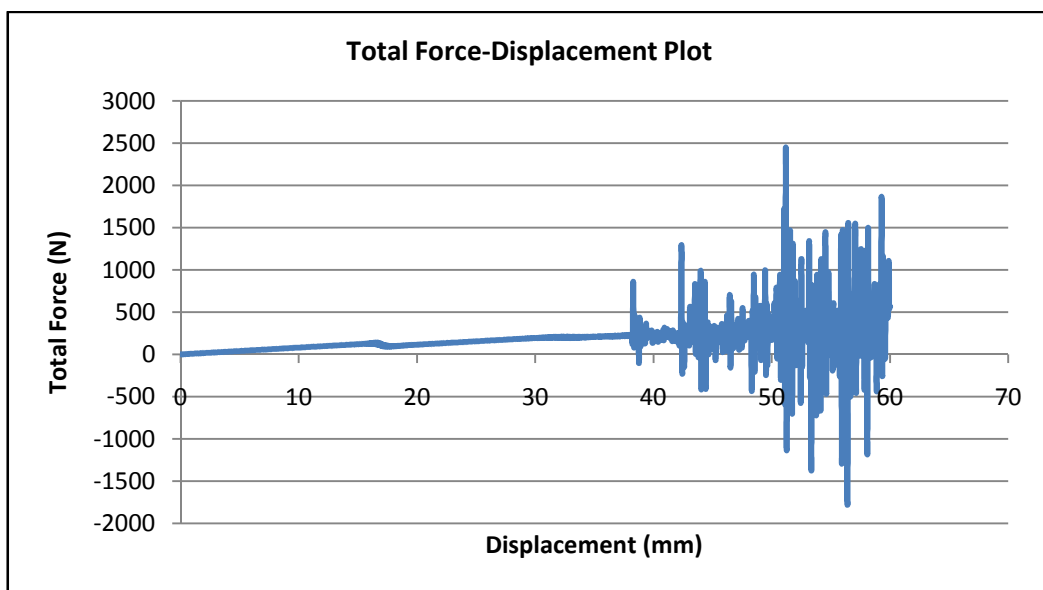

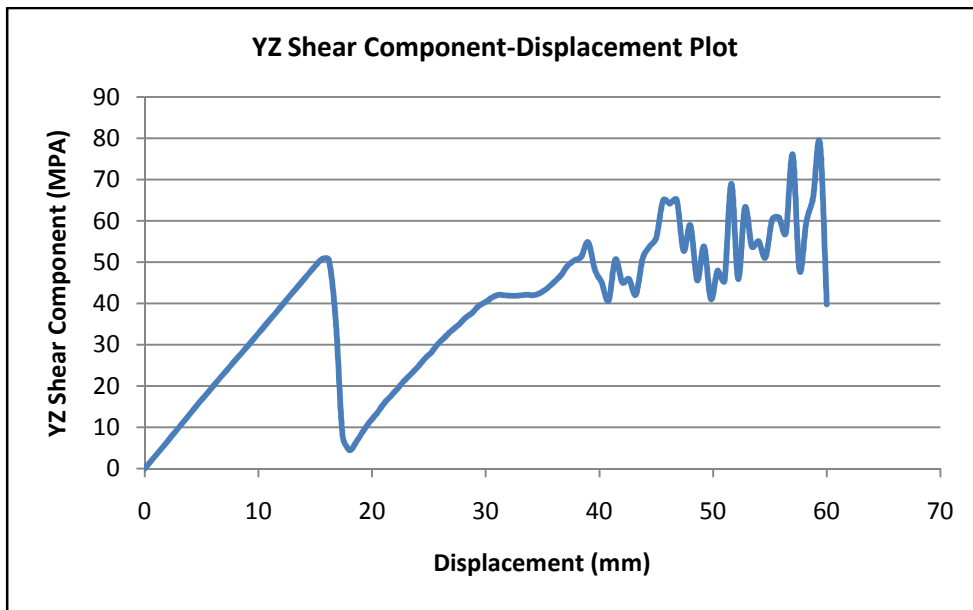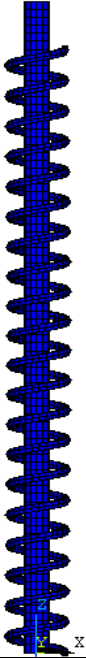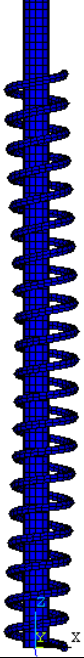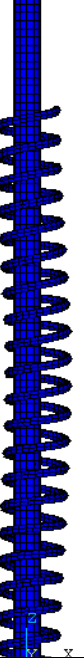**Figure 5.9.** Total Force Displacement Plot For Model 2

Figure 5.10. Total Force Displacement Plot For Model 2

Table 5.4. shows the deformed shapes and shear stress outputs from Model 2. Besides, shear stress results are also compared with each other. Model 2 gives almost the same deformed shapes as Model 1 gives. However, similar to Model 1, stress outputs are not close to analytical and theoretical results.

Similar to Figure 5.9, there is a sudden drop in the shear stress magnitudes between deformations of 15mm and 20mm. This is unexpected since deformation and shear stress magnitudes should be proportional. The reason of this behavior might be mistuned parameters. In order to find closer results, another model, Model 3, is constructed with additional damping.

Table 5.4. Model 2 Deformed Shape and Stress Output Comparison

Compression (mm)	20	40	60
Deformed Shape			
YZ Shear Stress-FEA-Average (MPa)	13	45	39
Analytical Shear Stress (MPa)	130	261	392
Experimental Shear Stress Results (MPa)	132	253	382

5.4.3 CONSTRUCTION OF MODEL 3 AND RESULT EVALUATION

For the third model, the same friction is kept as in Model 2. Additional damping is applied to the spring. Damping ratio of 2 is used and the results for highly damped system is obtained. Parameters used for this model used are FS=0.78, FD=0.42, VDC=20, and β=0.0168 (i.e. ξ=2). Force displacement curve is plotted in Figure 5.11. As Figure 5.11 is observed, force deflection character showed a linear pattern until there is contact between the rod and the spring. Besides, the slope of the line does not change between deformations between 15 and 20 mm. However, in Figures 5.7 and 5.9, there is a change of slope between those deformations. When those figures are compared with Figure 5.11, it is seen that the displacement at which oscillations start is shifted to deformations below 30 millimeters for Model 3. Addition of damping changes the critical buckling deformation. In Figure 5.12, YZ shear stress obtained from nodes is plotted versus time.

As Figure 5.12 is observed, it is seen that the amount of average shear stress in the node positions of interest show a linear pattern with increasing displacements. This behavior is expected since stress occurs as spring deforms. At deformations higher than 30mm, oscillations exist, which are caused due to contact between rod and the spring. Although stress amplitudes are still low with respect to experimental and theoretical values, they are more close to theoretical and

experimental results when compared to Model 1 and 2 results. Table 5.5 shows the obtained results. In Figures 5.8 and 5.10, stress amplitudes showed a sudden decrease between deformations of 15 and 20, which is not physical. Addition of damping removed this behavior.

Model 3 estimates buckling before the critical deformation obtained from analytical formulations. The deformed shapes are similar to the shapes obtained from experiment.
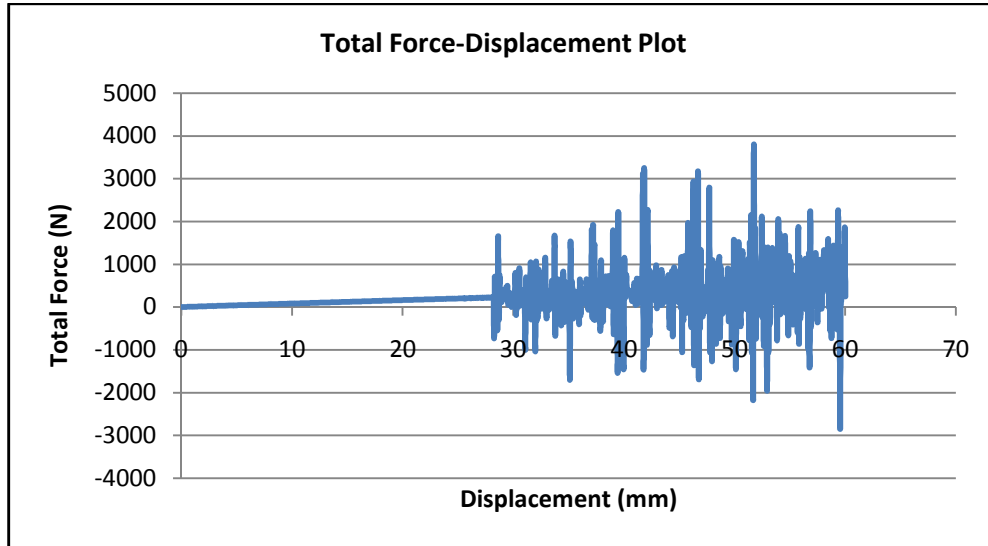

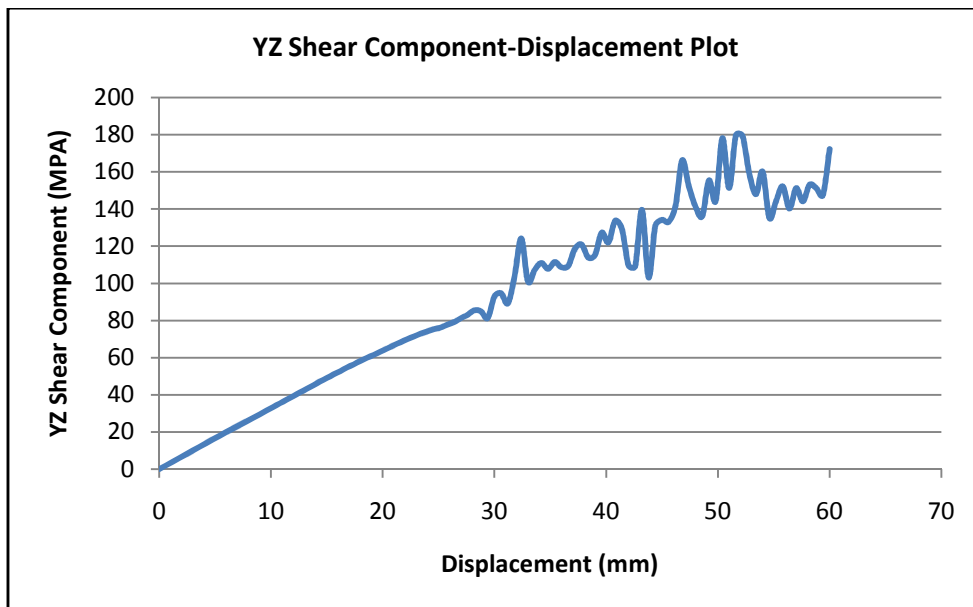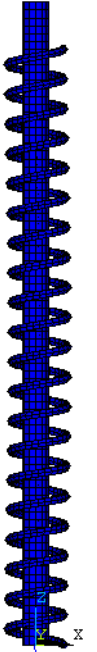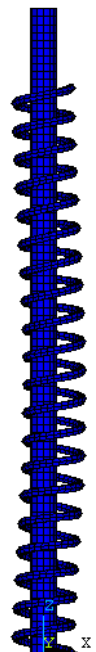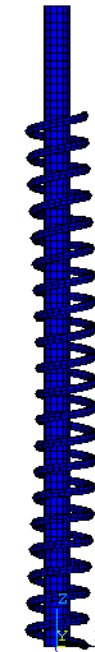**Figure 5.11.** Total Force Displacement Plot For Model 3

Figure 5.12. Total Force Displacement Plot For Model 3

Table 5.5. Model 3 Deformed Shape and Stress Output Comparison

Compression (mm)	20	40	60
Deformed Shape			
YZ Shear Stress-FEA-Average (MPa)	65	122	172
Analytical Shear Stress (MPa)	130	261	392
Experimental Shear Stress Results (MPa)	132	253	382

5.4.4 RESULTS COMPARISON

This section deals with comparing the results obtained in sections from 5.4.1 to 5.4.3 with the experimental results. Figure 5.13 and 5.14 shows the comparison of stress and force-deflection results with the ones obtained from experiment for Model 1. All plots presented in this section are obtained for compression phase of the experiment.

For Model 1, when Figures 5.13 and 5.14 are examined, it is seen that force deflection plot obtained from finite element analysis conforms with the one obtained from experiment. After contact is detected, oscillations start around the nominal value, which represents a linear spring behavior. On the other hand, the stress relation obtained from finite element analysis is far away from the experimental results.

Figure 5.13. Total Force Displacement Comparison Plot For Model 1

Figure 5.14. YZ Shear Stress Comparison For Model 1

For Model 2, when Figures 5.15 and 5.16 are examined, it is seen that force displacement plot obtained from finite element analysis conforms with the one obtained from experiment. After contact is detected, oscillations start around the nominal value, which represents a linear spring behavior. On the other hand, the stress relation obtained from finite element analysis is far away from the experimental results.

70

Figure 5.15. Total Force Displacement Comparison Plot For Model 2
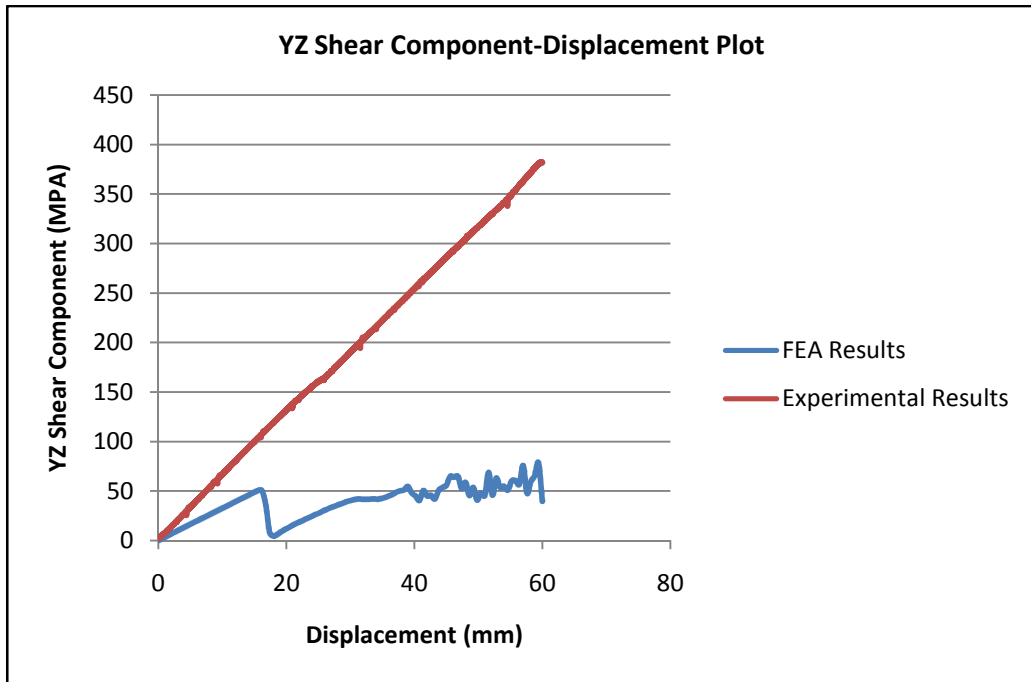
Figure 5.16. YZ Shear Stress Comparison For Model 2

For Model 2, when Figures 5.17 and 5.18 are examined, it is seen that force displacement plot obtained from finite element analysis conforms with the one obtained from experiment. After contact is detected, oscillations start around the nominal value, which represents a linear spring behavior.

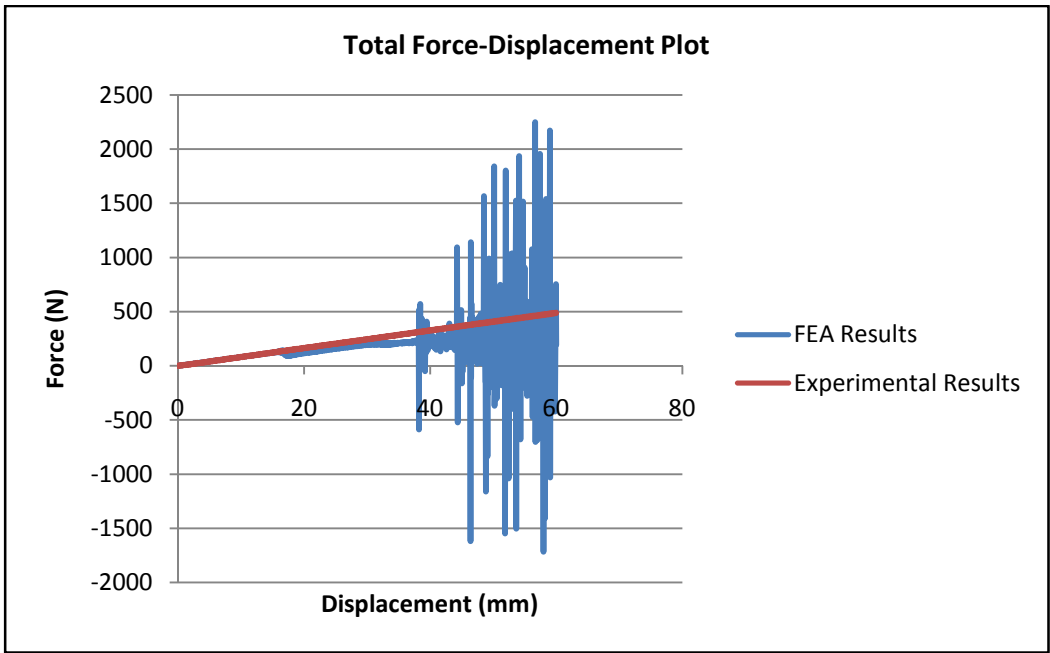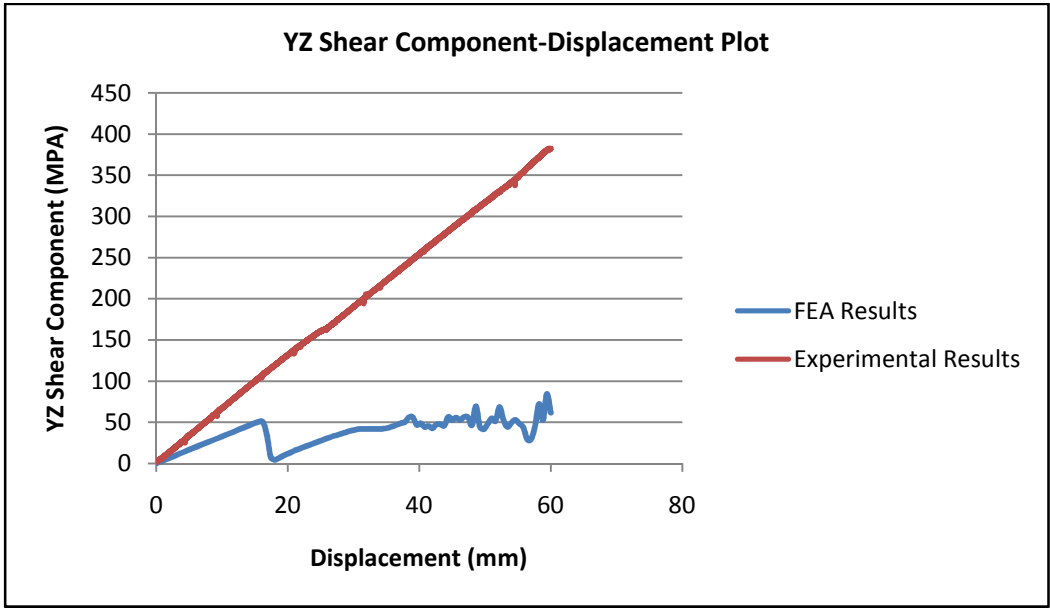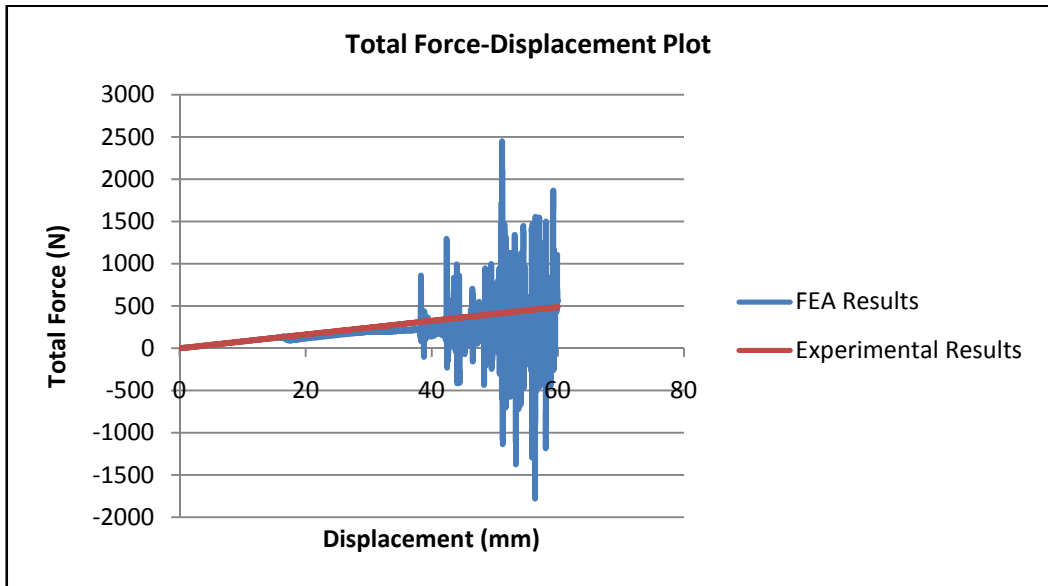On the other hand, the stress relation obtained from finite element analysis is far away from the experimental results. But still this model gives better results for stress magnitudes and trends when compared to previous models.
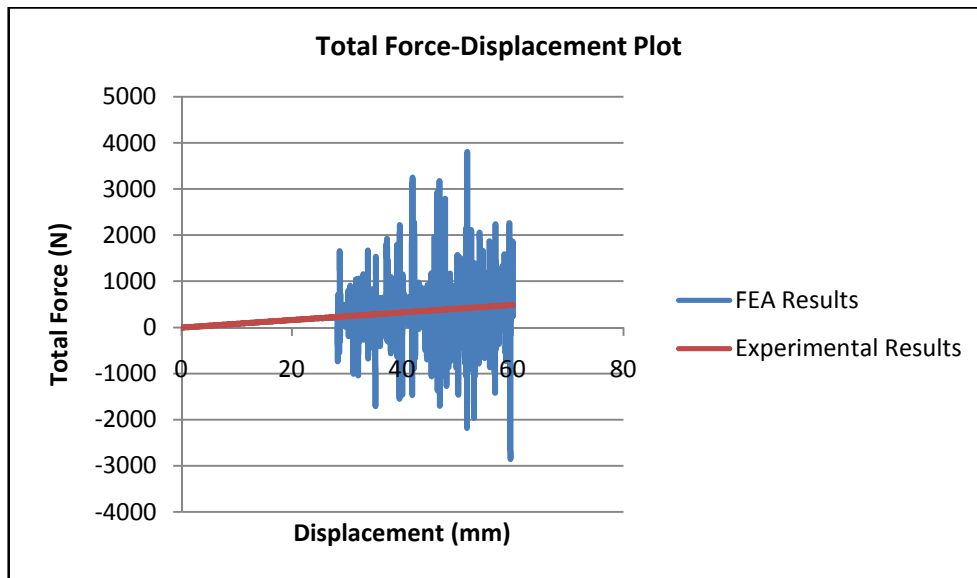

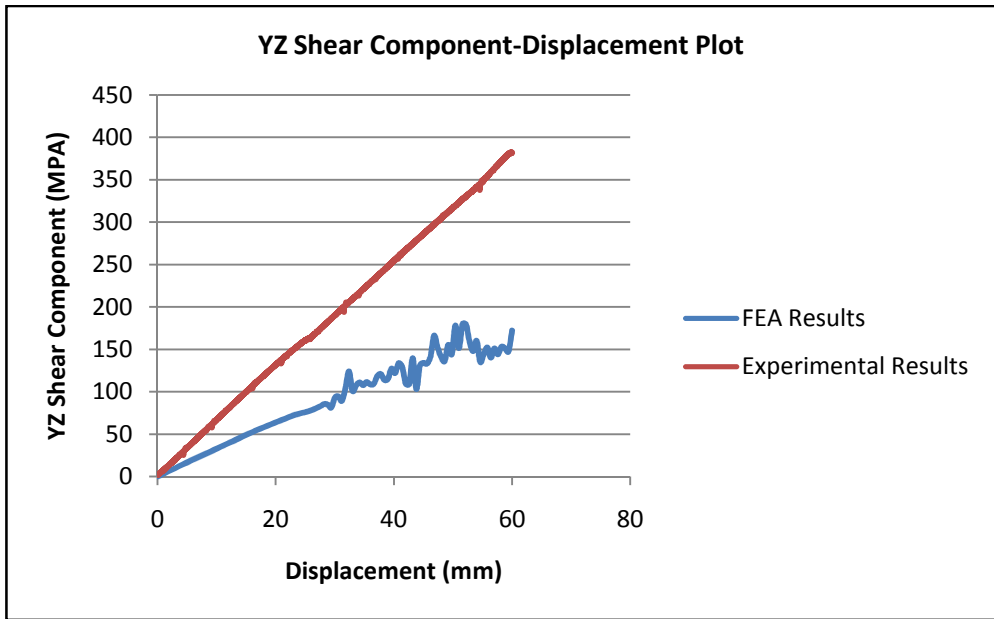**Figure 5.17.** Total Force Displacement Comparison Plot For Model 3

Figure 5.18. YZ Shear Stress Comparison For Model 3

CHAPTER 6

RESULT DISCUSSION AND CONCLUSION

Throughout this thesis study, it is aimed to provide a tool for the designer in order to analyze the recoil spring which is used in automatic weapons by using finite element methods. In addition to this, it is aimed to increase modeling knowledge of the recoil spring in finite element analysis. Effect of important parameters in finite element analysis such as contact, friction, damping definition, mesh size, boundary conditions, initial conditions are investigated and effect of each on stress and force displacement character is investigated.

Since motion of the spring involves contact and buckling, constructed model is made to cover those effects and give force-deflection characteristics and stress distribution in the recoil spring. For this purpose, two models are presented, namely Collision Model and the Simple Spring Model. The former is used if the breech hits the spring with a certain velocity in transient analysis and the latter is used if the deformation of the spring is known as a function of time.

During deformation of the recoil spring, reaction forces from the fixed nodes are extracted and used for force deflection characteristics derivation. Friction force is also collected by fixing the guiding rod by using a virtual node. This node is hold fixed and friction force is extracted from this node.

While modeling the spring, some amount of contact damping is applied in order to decrease the oscillations caused by the contact. Other kinds of material damping terms, such as the alpha and beta, are also applied on the spring to see their effect on the force deflection characteristics. However, damping showed no significant effect on the results obtained from the Collision Model. As the model is converted to simple spring model, those parameters effected both stress and force deflection characteristics.

Hence, it is important to mention that, boundary conditions can change the effect of parameters. For instance, damping seems to have no significant effect on the force-deflection characteristics for the Collision Model whereas, it effects the Simple Spring Model.

During this thesis study, an experiment is performed to see if the model parameters can be updated and made to give conforming results with the experiment. As damping value is increased, results come close to each other. Analysis results show a converging trend as damping ratio increase. However, it should be questioned if there really exist high damping in a mechanical system.

There is one possible explanation for this behavior. In the experiment, the spring is positioned on a seat and some amount of silicone adhesive is applied between spring and seat in order to prevent slippage. This material might have caused additional and unexpected damping to the system. Hence, as damping increase in the finite element model, the results seem to converge to each other. Therefore, as a future study, the experiment can be repeated without using any adhesive and results can be compared with a finite element model which only involves small amount of damping, such as material damping. This concludes that damping modeling is important for constructing an accurate finite element model in transient dynamic analysis. Damping effects stress outputs significantly.

Finite element models estimate the buckled geometry and the critical amount of deformation necessary for buckling. As the spring deforms and touches the guiding rod, oscillatory and non

linear behavior is observed both in stress and force displacement character. This is expected since contact means nonlinear behavior.

It is important to mention once more that, back and forth movement of the breech block is very fast, that is it occurs in milliseconds. Hence, experimental verification gives best results when those speeds are applied on the spring and high velocity cameras shall be involved for determination of deformed-buckled shape. Experiment performed in this study has low velocity when compared to the actual working condition. Hence, high speed experimentation is a future study that should be performed to see the validity of the models.

The experiment is performed with a data acquisition system which is capable of sampling frequency of 2000 Hz. This machine is used since the oscillations in the finite element solution at high deformation rates might be the response of the spring at high frequency. However, no oscillation is observed both for stress and force displacement outputs at the end of the experiment.

In the constructed models of section 5.4, model simulations show that, when the spring buckles and touches the guiding rod, it starts shaking in an unstable manner and contact condition changes continuously. Oscillations at higher compression amounts might have caused because of this motion. This is another evidence that, contact causes nonlinearities in the finite element model.

Stress outputs obtained from the experiment and the finite element analysis show difference. This may be caused because the maximum shear stress direction of the gage location may not coincide with the YZ shear stress direction of the finite element analysis. Since there is buckling and movement, those axis might not be aligned with each other.

By using the Collision Model and knowing the pressure distribution in the barrel, one can model the recoil mechanism and find the actual position of the block, consequently find the total cycle time. This is one of the future works that can be performed to advance this modeling study.

REFERENCES

[1]   Budynas-Nisbett, Shigley's Mechanical Engineering Design, 8th Edition, McGraw-Hill, 2008

[2]   United States Army Materiel Command, Engineering Design Handbook Automatic Weapons, pp 4-37, 1970

[3]   Handbook on Weaponry, Rheinmetall, pp 262-270, 1982

[4]   Handbook of the Thompson Machine Gun, Auto-Ordnance Corporation, 4th Edition, pp 3-4, 1929

[5]   Technical Description of the Automatic Rifle Hk G3, Heckler and Koch GMBH

[6]   M.V.Goncharenko, V.V.Goncharenko. Geometric Nonlinearity of Mechanical Behaviour As a Consequence of Large Deformations of Springs, Journal of Engineering Physics and Thermoplastics, Vol 82 No:6 , 2009

[7]   F.P.Beer, E.R. Johnston, J.T. Dewolf, Mechanics Of Materials, 4th Edition in SI Units, McGraw Hill, 2005

[8]   Engineering Design Handbook, Elements of Armament Engineering, Part Three, Weapon Systems and Components, 1963

[9]   M.Shimoseki, T.Hamano, T.Imaizumi, Fem For Springs, Japan Society For Spring Research, Springer, 2003

[10]   Y.Prawato, M.Ikeda, S.K.Manville, A.Nishikawa. Failure Analysis of Automotive Suspension Coil Springs, Association for Iron & Steel Technology Proceedings, pp 35-41 ,2008.

[11]   L.Lei, Shuguang Z., Xianwu Y., Jirui W., A Finite Element Analysis of the Barrel –shaped Helical Spring on the Vehicle Rear Suspension, International Conference On Computer Design And Applications (ICCDA), pp 115-117, 2010.

[12]   Husselman M., Modeling and Verification of Valve Train Dynamics in Engines, Master's thesis, University of Stellenbosch, 2005.

[13]   Mulla T.M., Kadam S.J.,Kengar V.S., Finite element Analysis of Helical Coil Compression Spring for Three Wheeler Automotive Front Suspension, International Conference on Mechanical and Industrial Engineering (IJMIE),Vol-2,2012, pp 74-77.

[14]   McWilson R.C, Stress Analysis and Fatigue Testing of Hermetic Compressor Suspension Spring, International Compressor Engineering Conference, pp 265-268, 1972.

[15]   Strain Gauge Installations, General Information, omega.co.uk

http://www.omega.co.uk/techref/pdf/Strain-gauge-application-info/strain-gauge-general-information.pdf

(Accessed 20 December 2012)

[16]   Strain Gage Thermal Output and Gage Factor Variation with Temperature, Tech Note TN-504-1, Micro measurements, Vishay Precision Group

[17]   Strain Gage Measurement-A Tutorial, Application Notes 078, National Instruments, 1998

[18]   Precise and Flexible Strain Gauges, Product Catalogue, Tokyo Sokki Kenkyujo Co, Ltd

[19]   Keller S.G, Gordon A.P. Equivalent Stress and Strain Distribution in Helical Compression Springs Subjected to Bending, Journal of Strain Analysis, Vol 46, pp 405-415, 2011

[20]   Mechanics of Materials Laboratory Instruction Material

         http://www.public.iastate.edu/~e_m.327/experiments/instructions/helspring.pdf

         (Accessed 23 December 2012)

[21]   ANSYS LS DYNA User's Guide, Release 12.0, Help System, Contact Technology Guide, Contact Definitions, ANSYS, Inc.

[22]   ANSYS Training Manual, Chapter 6 –Contact Surfaces

[23]   Ls-Dyna Support

         http://www.dynasupport.com/tutorial/contact-modeling-in-ls-dyna/contact-parameters

         (Accessed 23 December 2012)

[24]   ANSYS LS DYNA User's Guide, Release 12.0, Help System, Structural Analysis Guide, Transient Dynamic Analysis Options, Damping, ANSYS, Inc.

[25]   Avallone E.A., Baumeister T., Sadegh A.M. Mark's Standard Handbook For Mechanical Engineers, 11th Edition, Mc Graw Hill, 2006

[26]   ANSYS LS DYNA User's Guide, Release 12.0, Help System, Element Reference, ANSYS, Inc.

APPENDIX A

STRAIN GAGE AND STRESS FORMULAE

Strain gage is a sensor which relies on the proportional variance of electrical resistance to strain, hence it is used to measure strain on the bonded surface The wire inside the gage, extends or contracts according to the applied load, which causes a change in resistance of the metallic wire. The relation between wire resistance and strain is linear. Figure A1 shows a simple strain gage. The amount of strain is found by detecting amount of resistance change. In order to determine this change, strain gages are used in Wheatstone bridge, in which four resistances are connected to an external power supply as shown in Figure A2. There are other kinds of connection types, but only quarter bridge configuration is mentioned for the scope of this study.
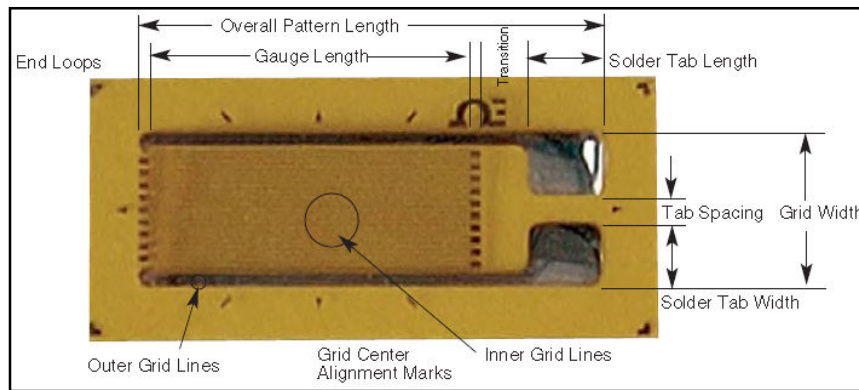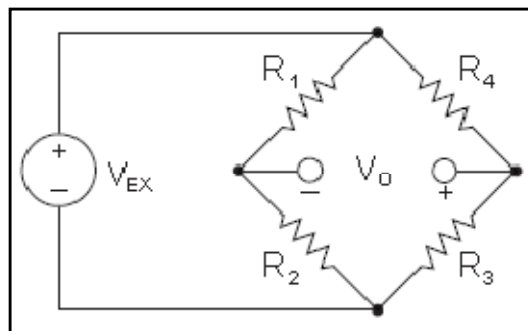

Figure A1. Metallic Wire Strain Gage [15]

Figure A2. Quarter Wheatstone Bridge [17]

From Figure A2, the bridge is said to be in equilibrium if V_0 is zero. If the gage experiences any strain, output voltage will be nonzero and the balance is disturbed. After application of the strain gage, the bridge takes the form in Figure A3, the equation between voltage difference and the strain is given by Equation A1 if $R_1=R_2$ and $R_3=R_G$

After each strain in the three element strain gage rosette is found by using Equation A1, stress magnitudes are evaluated by using Equations A2 to A4 according to the convention shown in Figure A4.
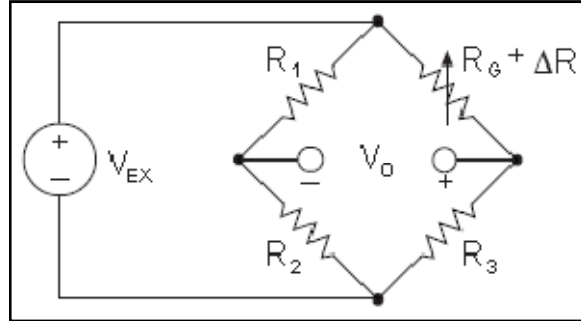

Figure A3. Quarter Wheatstone Bridge- Gage Resistance [17]

$$\frac{V_0}{V_{ex}} = -\frac{GF \times \varepsilon}{4} \left\{ \frac{1}{1 + GF \times \frac{\varepsilon}{2}} \right\} \tag{A1}$$
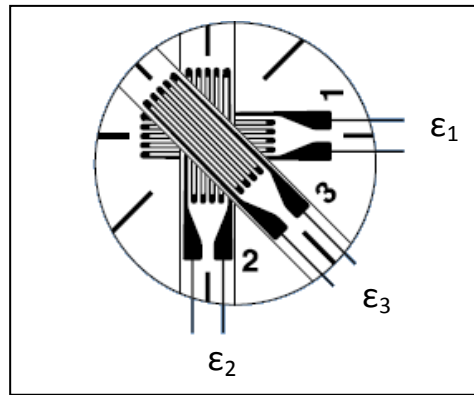

Figure A4. Three Element Strain Rosette[17]

$$\sigma_{max} = \frac{E}{2} \left[\frac{\varepsilon_1 + \varepsilon_2}{1 - \nu} + \frac{1}{1 + \nu} \sqrt{2\left\{ \left(\varepsilon_1 - \varepsilon_3\right)^2 + \left(\varepsilon_2 - \varepsilon_3\right)^2 \right\}} \right] \tag{A2}$$

$$\sigma_{min} = \frac{E}{2} \left[\frac{\varepsilon_1 + \varepsilon_2}{1 - \nu} - \frac{1}{1 + \nu} \sqrt{2\left\{ \left(\varepsilon_1 - \varepsilon_3\right)^2 + \left(\varepsilon_2 - \varepsilon_3\right)^2 \right\}} \right] \tag{A3}$$

$$\tau_{max} = \frac{E}{2(1+v)}\left[\sqrt{2\left\{\left(\varepsilon_1 - \varepsilon_3\right)^2 + (\varepsilon_2 - \varepsilon_3)^2\right\}}\right] \qquad (A4)$$

APPENDIX B

SAMPLE CALCULATIONS

In this section, one sample calculation is shown for finding the stress for 40 millimeter of compression on the spring. Below calculations are performed for the case of 40 millimeter's deformation. The values obtained from the set up at the 40 millimeter deformation is given in Table B1.

Table B1. Gage Outputs

Gage Number	1	2	3
Voltage (V)	-1.122	0.895	-0.404

By using Equation A1, the corresponding strain values are evaluated and shown in Table B2.

Table B2. Strain Counterparts

Gage Number	1	2	3
Channel Gain	250	250	250
Gauge Factor	2.14	2.14	2.14
Strain	1.68×E-3	-1.33×E-3	6.04×E-4

After finding the strains, maximum stresses are found by using Equations A2 through A4 and the material properties given in Table 3.3. Results are shown in Table B3.

Table B3. Principal Stresses

σmin (MPa)	-200
σmax (MPa)	302
τmax (MPa)	251